scientific reports

Check for updates

OPEN

Computational identification of PDL1 inhibitors and their cytotoxic effects with silver and gold nanoparticles

Syed Hammad Ali[1], Hiba Ali[2] & Mohd. Azhar Aziz[1,3]✉

Immunotherapy is a promising treatment for cancer that aims to boost the immune system's response to cancer cells. This can be achieved by blocking Programmed cell death protein 1/Programmed death-ligand 1 (PD1/PDL1), which activates T cells. In this work, the aim was to find high-affinity drugs against PDL1 using computational tools and conjugate nanoparticles with them. The cytotoxic activity of the nanoparticle conjugated drugs was then tested. The screening of 100,000 drugs from the ZINC database and FDA-approved drugs was done computationally. The physicochemical properties and toxicity of the drugs were analyzed using SwissADME and ProTox-II, respectively. Silver nanoparticles (AgNPs) and gold nanoparticles (AuNPs) were synthesized using extracts of *Catharanthus roseus* flowers and *Juglans regia* shells, respectively. The characterization of AgNPs and AuNPs was performed using UV–Vis spectroscopy, X-ray diffraction (XRD), and Fourier transform infrared spectroscopy (FTIR). Their conjugation with the drugs Irinotecan, Imatinib, and Methotrexate was also confirmed using UV–Vis, FTIR, and Dynamic light scattering (DLS). The top screened drugs were ZINC1098661 and 3 FDA-approved drugs (Irinotecan, Imatinib, and Methotrexate). Docking studies revealed that Irinotecan had the highest binding affinity towards PDL1 when conjugated with silver nanoparticles (AgNPs) and gold nanoparticles (AuNPs). The Irinotecan-PDL1 complex was confirmed as the most stable through molecular dynamics simulations. The result of the methylthiazol tetrazolium (MTT) assay showed that conjugated AgNPs and AuNPs with Irinotecan had a higher toxic effect on the A549 cancer cell line than AgNPs and AuNPs conjugated with Imatinib. This study provides a promising avenue for further investigation and development of nanoparticle-drug conjugates as a potential cancer immunotherapy strategy.

Keywords Immunotherapy, MTT assay, Molecular dynamics simulations, Nanoparticles, PD1/PDL1 immune checkpoint, T cells activation

Abbreviations

AuNPs	Gold nanoparticles
AgNPs	Silver nanoparticles
DLS	Dynamic light scattering
FTIR	Fourier transform infrared spectroscopy
MD simulation	Molecular dynamics simulation
MTT	Methylthiazole tetrazolium
PDB	Protein data bank
PD1	Programmed cell death 1
PDL1	Programmed death-ligand protein 1
Rg	Radius of gyration
RMSD	Root mean square deviation
RMSF	Root mean square fluctuation
SASA	Solvent accessible surface area
TEM	Transmission electron microscopy

[1]Interdisciplinary Nanotechnology Centre, Aligarh Muslim University, Aligarh, UP 202002, India. [2]Interdisciplinary Biotechnology Unit, Aligarh Muslim University, Aligarh, India. [3]Cancer Nanomedicine Consortium, Aligarh Muslim University, Aligarh, India. ✉email: azhar.inc@amu.ac.in

UV–Vis spectroscopy	Ultraviolet–visible spectroscopy
XRD	X-ray diffraction

Cancer is a devastating disease due to which millions of deaths occur every year worldwide[1]. According to the statistical report by the World Health Organization (WHO), 10 million people died from cancer in 2020, and the most occurring cancer was breast and lung cancer[2]. In the treatment of cancer, chemotherapy is one of the most adopted treatments. However, it has several limitations, such as drug resistance issues[3], as well as side effects such as hair loss, constipation[4], and adverse effects on normal cells[5].

Recently, immunotherapy has emerged as a more advanced and promising approach to cancer treatment[6]. In immunotherapy, the immune system is enhanced by modification in immune cells to target cancer cells that are evaded by the immune system[7]. Currently, research is also going on cancer immunotherapy using nanomedicine, such as nanoparticles, to treat cancer by targeting delivery[8]. Moreover, targeting the Programmed cell death protein 1/Programmed death-ligand 1 (PD1/PDL1) immune checkpoint is a widely studied cancer immunotherapy[9]. PDL1, which is also known as CD279 and B7-H1, is a membrane protein that is considered a cancer biomarker. The extracellular region of PDL1 consists of IgV and IgC domains. It belongs to the B7 series and has a 33-kDa type 1 transmembrane glycoprotein with 290 amino acids[10]. There is an overexpression of the PDL1 receptor on cancer cells, which binds with PD1. This interaction causes the deactivation of T cells, leading to tumor growth[11]. Targeting PDL1 can inhibit interaction with PD1 to prevent immunosuppression; for example, PDL1 is targeted by various nanoparticles and nanoparticles conjugated with drugs[12–14].

Nanoparticles (NPs) are materials with dimensions on the nanoscale ranging from 1 to 100 nm[15]. They can be synthesized by physical, chemical, and biological methods[16]. There are several advantages of the biological synthesis of nanoparticles over chemical synthesis, such as low toxicity and high biocompatibility, therefore, it is very significant to use them in healthcare applications[17]. Moreover, biological materials can also provide natural compounds which enhance the efficiency of nanoparticles. According to the WHO, herbal sources possess medicinal properties to treat diseases[18]. For example, the *Catharanthus roseus* plant has seven anti-cancer compounds, which are vincristine, vinblastine, vindogentianine, vindolidine, vindoline, vindolinine, and vindolicine[19]. Additionally, *Juglans regia* is rich in vitamins E, folate, melatonin, various antioxidative polyphenols, and ω-3 fatty acids[20]. Moreover, studies have shown that *Juglans regia* can slow the growth and angiogenesis of colon and renal cancer[21].

Nanoparticles are suitable for drug loading because they have a high surface area due to their size in the nano range. This also improves the stability and hydrophilicity of drugs for drug delivery[22,23]. For example, silver nanoparticles (AgNPs) conjugated with doxorubicin can be effective in killing cancer cells[24], and gold nanoparticles (AuNPs) can be conjugated with doxorubicin to target PDL1[25]. For the treatment, nanoparticles conjugated with a drug can be taken through oral, nasal, parenteral, or intraocular routes[26].

These days, in silico drug screening is an excellent approach for discovering new drugs, particularly when screening millions of chemical compounds, which is very hard to do in a wet lab[27]. Additionally, molecular dynamics simulations can help to predict the behavior of drugs with protein receptors, which can be useful for analyzing their stability[28].

There are various Food and Drug Administration (FDA) approved monoclonal antibody drugs available to inhibit PD1/PDL1, such as Nivolumab and Durvalumab[29,30]. However, these macromolecular antibody drugs may not be effectively able to penetrate cancerous cells[31]. Moreover, manufacturing monoclonal antibodies is a difficult and expensive process, and storing and transporting them is also very challenging[32]. Therefore, there is a need to discover new small inhibitors that can target the PD1/PDL1 immune checkpoint pathway to overcome these limitations. Currently, various small molecule drugs, such as JQ1 and CA-170, are under clinical research to evaluate their safety and efficacy in treating cancer[31].

In this study, 100,000 compounds retrieved from the ZINC database were screened against PDL1 (accession code 5C3T) in order to identify the compounds with the highest binding affinity with PDL1 to block the interaction between PDL1 and PD1. Further, screened compounds were arranged on the basis of affinity score. Subsequently, 7 FDA-approved compounds were again filtered based on low steric hindrance. Then, top drugs Irinotecan, Imatinib, Methotrexate, and ZINC1098661 were filtered out for more analysis based on Absorption, Distribution, Metabolism, and Excretion (ADME) properties, Lipinski's rule of five, carcinogenicity, and cytotoxicity. The structural analysis was also done to reveal the binding site and interaction of PDL1 with drugs. Moreover, the binding energy of selected drugs with AgNPs and AuNPs against PDL1 was also analyzed. Furthermore, the stability of PDL1 with drugs and their conformational changes were analyzed by performing molecular dynamics simulations in a solvent condition for 10 ns for each drug, and 100 ns specifically for Irinotecan. In the lab, the filtered-out drugs were conjugated with synthesized AgNPs and AuNPs mediated by *Catharanthus roseus* and *Juglans regia,* respectively. Subsequently, the drugs, nanoparticles, and nanoparticles conjugated with drugs were tested on the A549 cell line for comparative studies.

Materials and methods

In silico analysis

Virtual tools and resources

The 3D structure of PDL1 was retrieved from the Research Collaboratory for Structural Bioinformatics Protein Data Bank (RCSB PDB) using the accession code 5C3T, and a database containing 100,000 ligand compounds was obtained from the ZINC database. PyRx, Autodock Vina, and 3D QSAR were used for the virtual screening of drugs. The CHARMM-GUI was used for designing nanoparticles and their docking performance was evaluated using Hex 8.0.0. SwissADME and ProTox-II were utilized for analyzing the properties and toxicity of drugs respectively. MD simulation studies were performed using GROMACS on an Asus ROG laptop equipped with a Core i7 processor, 32 GB of RAM, and a 4 GB NVIDIA GTX 1650 Ti graphic card.

Multiple drug docking using PyRx and AutoDock Vina
Multiple drug docking was performed using PyRx, utilizing the random forest machine learning algorithm[33]. The database was converted into the PDBQT format, and energy minimization was carried out before starting the docking process. For further filtration, the selected drugs were then docked using AutoDock Vina, with the use of a genetic algorithm[34]. Heteroatoms were removed, and energy minimization was performed, followed by the addition of polar hydrogen and Kollman charges. The grid parameters were set to 68, 70, and 104, centralized at 6, 12, and 8 for the X, Y, and Z coordinates, respectively, with a grid spacing of 0.5 Å and an exhaustiveness of 8. The docking was carried out based on high affinity. PyMOL was used to visualize the docked structure of protein and ligand complex[35].

3D QSAR (quantitative structure–activity relationship) for a further selection of drugs
The FDA-approved drugs underwent further analysis using a Three-Dimensional Quantitative Structure–Activity Relationship (3D QSAR) in order to pinpoint compounds with higher experimental activity[36]. The drugs were loaded into a 3D QSAR server, with Half-Maximal Inhibitory Concentration (IC_{50}) values for each drug being retrieved from the ChEMBL database[37]. The 3D QSAR model dataset was created by conducting a conformational analysis of the molecules with the innovative balloon method while aligning the molecules through the use of the RDKit method. Finally, the 3D QSAR model was generated using the Comparative Molecular Field Analysis (CoMFA) method.

Docking with AgNPs and AuNPs
The selected drugs were docked with silver and gold nanoparticles designed using Chemistry at HARvard Macromolecular Mechanics—Graphical User Interface (CHARMM-GUI) modulator[38]. The size of the nanoparticles was set at 35 nm. The docking process was carried out using Hex 8.0.0, with the protein and conjugated nanoparticles with drugs being loaded into the software[39]. The algorithm used for the process was the Geometric Hashing and Energy Minimization algorithm. The docking process was initiated once these structures were loaded.

Predicting physicochemical properties and toxicity of compounds
The selected compounds were analyzed for their physical and chemical characteristics using the SwissADME, with a particular emphasis on whether they comply with Lipinski's rule of five[40]. In addition, the compounds were assessed for their potential to induce cytotoxicity and carcinogenicity using the ProTox-II tool to ensure their safety[41].

Molecular dynamics simulations
The system was prepared for simulation by creating a protein topology file using GROningen MAchine for Chemical Simulations (GROMACS). The PRODRG was then used to generate a topology file for the ligand[42]. The GROMOS96 43a1 force field was chosen to describe the interactions between the atoms in the system[43]. A cubic box was generated to contain the system, and water molecules were added to the box to create an aqueous environment. To neutralize the charge of the system, Na^+ and Cl^- ions were added. The steepest descent method was used to minimize the energy of the system and eliminate any unnecessary steric clashes for a duration of one nanosecond and a total of 50,000 steps. During both the NPT (constant pressure and temperature) and NVT (constant volume and temperature) equilibration phases, a temperature of 300 K and a pressure of one bar were maintained using periodic boundary conditions throughout the simulation. A 10 ns molecular dynamics simulation was performed using GROMACS to study the interaction between PDL1 and Irinotecan, Imatinib, Methotrexate, and ZINC1098661. Additionally, a 100 ns molecular dynamics simulation was specifically conducted for Irinotecan[44]. The simulation was performed using the Particle Mesh Ewald (PME) method to calculate long-range electrostatic interactions[45]. The resulting trajectories from the simulation were analyzed using the inbuilt utilities of GROMACS and visualized using Visual Molecular Dynamics (VMD) and XMGRACE software[46,47].

Synthesis of AgNPs and AuNPs
In order to synthesize silver nanoparticles, 20 g of fresh *Catharanthus roseus* flowers were washed and added to a flask containing 200 ml of deionized water (dd H_2O). The mixture was boiled to obtain the extract of the flowers, which was then allowed to cool to room temperature. A solution of silver nitrate was made by dissolving 17 mg of silver nitrate powder (Brand RANKEM, Product Code: S0080) in 100 ml of deionized water. The flower extract and silver nitrate solution were then mixed in a 9:1 ratio to initiate the synthesis of silver nanoparticles. Furthermore, to synthesize gold nanoparticles, 20 g of *Juglans regia* shells were taken in a separate flask containing 200 ml of deionized water. The flask was boiled to get an extract of shells. A 1.0 M solution of Gold (III) chloride hydrate ($HAuCl_4$) (Brand CDH, CAS No. 16961-25-4) was prepared by dissolving 1.0 g of $HAuCl_4$ in 25 ml of deionized water. The extracts of shells were mixed with 1.0 mM $HAuCl_4$ solution in separate flasks in a 4.5:0.5 ratio to start the synthesis of gold nanoparticles.

Characterization of AgNPs and AuNPs
Visible spectral analysis
The absorbance peaks of the AgNPs and AuNPs were measured using a spectrophotometer. A Carry 5000 UV–Vis NIR spectrophotometer (Agilent Technologies) was used. The Surface Plasmon Resonance (SPR) absorption of AgNPs is typically observed in the range of 400 to 800 nm, while the SPR absorption of AuNPs is typically observed in the range of 520 to 570 nm[48,49].

X-ray diffraction (XRD) analysis
The crystal structure and morphology of the AgNPs and AuNPs were confirmed through XRD analysis. The samples were dried on glass slides and prepared for analysis. Rigaku MiniFlex II XRD machine was used to perform XRD. The diffraction pattern of the sample was measured at 2°θ intervals from 30° to 80°[50].

Fourier transform infrared (FTIR) analysis
FTIR spectroscopy was used to identify the functional groups present on the surface of AgNPs & AuNPs. KBr (potassium bromide) was used as a matrix in FTIR spectroscopy, and a small amount of the sample was mixed with it to form a mixture. The mixture was then pressed into a pellet and placed in the sample compartment of an FTIR spectrometer. The PerkinElmer FTIR instrument was utilized to obtain the FTIR spectrum of the AuNPs and AgNPs, with measurements conducted within the wavenumber range of 500–4000 cm^{-1}[51].

Drug preparation and nanoparticles drugs conjugation

Irinotecan, Imatinib, and Methotrexate were obtained from the Jawaharlal Nehru Medical College (JNMC) in Aligarh. 100 mg of Imatinib and Methotrexate were weighed and crushed into a powder form. The powdered drugs were then placed in two separate flasks, each containing 100 ml of deionized and autoclaved water. The Whatman filter paper was used to filter the solution. Then, 5 ml of silver nanoparticles and 5 ml of gold nanoparticles were separately mixed with 125 µl (20 mg/ml) of Irinotecan to create solutions with a final drug concentration of 0.5 mg/ml for each solution. Additionally, 5 ml of silver nanoparticles and 5 ml of gold nanoparticles were also separately mixed with 5 ml (1 mg/ml) of Imatinib and 5 ml (1 mg/ml) of Methotrexate, respectively, to create solutions for each with a final drug concentration of 0.5 mg/ml. The mixture was stirred and left at room temperature for 48 h. The solutions were then centrifuged at 6000 rpm for 15 min, and the supernatant was discarded. The drugs were loaded again and centrifuged. The supernatant containing unbound drugs was discarded, and the pellet for each drug was collected.

Characterization of drugs conjugated with AgNPs and AuNPs

Visible spectral analysis
After drug conjugation, the optical densities (ODs) of the nanoparticles conjugated drugs were measured using a spectrophotometer. Slight variations in the maximum absorbance peaks were observed in both AgNPs and AuNPs, which confirmed that the nanoparticles had not undergone any changes in shape or structure after conjugation. The measurements were carried out utilizing an Agilent Technologies Instrument Carry 5000 UV–Vis NIR spectrophotometer[52].

Fourier transform infrared (FTIR) analysis
FTIR analysis was performed to examine the conjugation between drugs with AgNPs and AuNPs. The liquid samples were prepared for FTIR analysis using a previously described method. To obtain the Fourier transform infrared (FTIR) spectrum of the nanoparticles conjugated with the drugs, the PerkinElmer instrument was utilized. The measurement was conducted within the wavenumber range of 500–4000 cm^{-1}[53].

Dynamic light scattering (DLS) analysis
Dynamic light scattering was used to determine the size distribution of AgNPs and AuNPs before and after they were conjugated with tested drugs. The average size (d.nm) of the solutions was measured[54].

In vitro analysis

Cell culture
A549, a lung cancer cell line, was purchased from the National Centre for Cell Science (NCCS) in Pune. The medium used for cell culture was Dulbecco's Modified Eagle's Medium (DMEM, AL007S-Himedia), which was supplemented with 10% fetal bovine serum (FBS, RM10434-Himedia) and 1% penicillin–streptomycin (Pen-Strep, A004-Himedia). The cells were cultured in a T15 flask containing 5 mL of media in an incubator with 5% CO_2, 95% humidity, and a temperature of 37 °C. The medium was refreshed every other day.

Cytotoxicity assay
Twelve samples were analyzed using the methylthiazol tetrazolium (MTT) assay (Promega CellTiter 96® Aqueous, G3582), a colorimetric assay, to evaluate the effectiveness of drugs (0.5 mg/ml), AgNPs (0.1 mg/ml), AuNPs (0.1 mg/ml), and AgNPs and AuNPs conjugated with drugs (0.25 mg/ml). The MTT assay used a solution of 3-(4,5-dimethylthiazol-2-yl)-2,5-diphenyltetrazolium bromide dye to assess the samples. A T15 flask containing 80% confluent A549 cells (with a cell number of 1.12×10^6) was used for performing the MTT assay. The medium was removed, and the cells were washed with phosphate buffer saline (PBS). The cells were trypsinized using 0.5 ml of EDTA trypsin and incubated for 2 min in an incubator at 37 °C to detach them from the surface of the T15 flask. The cells with EDTA trypsin were centrifuged at 2000 rpm for 2 min, and the supernatant was discarded. The obtained pellet was resuspended in 1 ml of media. Subsequently, 0.7 ml of the cell suspension containing 7.84×10^5 cells was carefully drawn from the 1 ml resuspended solution and mixed with 9.6 ml of fresh media. Finally, 100 µl of the cell suspension containing 7840 cells was delicately seeded into each well of a 96-well plate. Then, 100 µl of each of the test samples was seeded in triplicate wells. In well A, untreated cells were used as a control, and three drugs (Irinotecan, Imatinib, and Methotrexate) were also included. In well B, AgNPs and their drug conjugates were seeded, and in well C, AuNPs were seeded along with their drug conjugates. The 96-well plate was incubated at 37 °C for 24 h in a humidified, 5% CO_2 atmosphere. After 24 h, 20 µl of MTT Reagent was added to each well that contained samples. The culture plates were then

S.No.	Compound	Affinity (kcal/mol)
1	ZINC1098661	−7.7
2	ZINC5832159	−7.5
3	ZINC8782706	−7.0
4	ZINC20638084	−6.9
5	ZINC20637343	−6.8
6	ZINC20637348	−6.8
7	ZINC20638090	−6.7
8	ZINC20638060	−6.5
9	ZINC20638066	−6.2
10	ZINC215892771	−5.8

Table 1. List of docking scores of 10 compounds using AutoDock Vina.

S.No.	Compound	Affinity (kcal/mol)
1	Irinotecan	−8.4
2	Sorafenib	−7.9
3	Imatinib	−7.8
4	Methotrexate	−7.4
5	Exemestane	−7.2
6	Lenvatinib	−7.2
7	Stivarga	−7.1

Table 2. List of the 7 top-hit FDA-approved drugs using AutoDock Vina.

incubated at 37 °C in a humidified, 5% CO_2 atmosphere for 3 h. After incubation, a 96-well plate, Enzyme-Linked Immunosorbent Assay (ELISA) plate reader, was used to record the absorbance at 490 nm.

Results

PyRx & AutoDock Vina docking analysis

The PyRx docking tool was used to select the top 10 hits chemical compounds with high affinity for the PDL1 protein from a database of 100,000 drugs. These compounds had an affinity ranging from −10.3 to −10.7 kcal/mol (Supplementary Table S1).

Next, the primary lead compound, ZINC1098661, was selected from the 10 chemical compounds based on its higher affinity of −7.7 kcal/mol, as determined by AutoDock Vina (Table 1).

The high docking score of ZINC1098661 among all 10 compounds using AutoDock Vina revealed that it shows the best affinity, with the interaction between ZINC1098661 and PDL1 via hydrogen bonding and electrostatic interactions.

In addition, the top 28 FDA-approved drugs with high affinity for PDL1 protein were also selected using the PyRx docking tool, which had affinities ranging from −6.4 to −10.8 kcal/mol (Supplementary Table S2).

Irinotecan has the highest affinity among all drugs, which suggests that its interaction is more stable with PDL1, i.e., its binding to the protein and the shape of Irinotecan leads to low-energy binding, resulting in high affinity.

Then, among these FDA-approved drugs, the 7 drugs with higher affinities in the range of −7.1 to −8.4 kcal/mol were selected using AutoDock Vina (Table 2). Among all 7 compounds, Irinotecan showed a high affinity of −8.4 kcal/mol, revealing that hydrogen bonding and electrostatic interactions between Irinotecan and PDL1 are the most stable. In the initial filtration, Sorafenib affinity was lower than Imatinib, but in the second filtration, it showed higher affinity in comparison with Imatinib with a difference of 0.1 (kcal/mol). This suggests that Sorafenib showed slightly better stable binding with PDL1 amino acid residues after interaction with polar hydrogen and electrostatic interactions. However, all 7 compounds were considered for 3D QSAR analysis.

3D QSAR analysis

The 7 FDA-approved drugs, which were previously selected by AutoDock Vina, were further filtered using 3D QSAR analysis. The resulting three drugs, Irinotecan, Imatinib, and Methotrexate, were selected based on experimental values generated by the 3D QSAR model, which depends on steric hindrance between cellular components and the drugs. Drugs with lower steric hindrance have higher experimental values. (Table 3).

Analysis of physicochemical properties and toxicity of drugs

Irinotecan, Imatinib, Methotrexate, and ZINC1098661 have almost passed Lipinski's rule of five, indicating that they are likely to be effective and safe for use (Table 4). However, Irinotecan has one violation, which is that its molecular weight exceeds 500 Da.

S.No.	Compound	Experimental value
1	Irinotecan	8.23
2	Methotrexate	8.20
3	Imatinib	8.15
4	Exemestane	8.13
5	Stivarga	8.11
6	Sorafenib	8.10
7	Lenvatinib	8.09

Table 3. List of the 7 FDA-approved drugs using 3D QSAR analysis.

Compound	Molecular weight (Da)	No. rotatable bonds	No. H-bond donor	No. H-bond acceptor	LogP	Lipinski violation
Irinotecan	586.68	6	1	8	4.95	1
Imatinib	493.6	8	2	6	4.04	0
Methotrexate	454.44	10	5	9	1.01	0
ZINC1098661	288.30	1	2	2	1.79	0

Table 4. The physicochemical properties of four potentially selective compounds.

Compound	Toxicity		GI absorption	Bioavailability
	Cytotoxicity	Carcinogenicity		
Irinotecan	Inactive	Inactive	High	0.55
Imatinib	Inactive	Inactive	High	0.55
Methotrexate	Inactive	Inactive	Low	0.11
ZINC1098661	Inactive	Inactive	High	0.55

Table 5. Toxicity, GI absorption, and bioavailability score of the selected compounds.

The Logarithm of the Partition Coefficient (logP) values for all the drugs in this group are less than 5, indicating that they are soluble in water. Additionally, tests for cytotoxicity and carcinogenicity showed that these drugs had low toxicity (Table 5). The gastrointestinal (GI) absorption and bioavailability scores for Irinotecan, Imatinib, and ZINC1098661 were higher than Methotrexate. This suggests that these drugs may have better oral absorption and effectiveness compared to Methotrexate.

Analysis of drugs conjugated with PDL1 receptor

The Irinotecan, Imatinib, Methotrexate, and ZINC1098661 hydrophobic interaction with the PDL1 domain is shown in (Fig. 1), and. Specifically, the residues Pro24, Lys25, and Lys41 of the PDL1 protein are found to interact with Irinotecan, while Lys25, Asp26, Tyr28, and Val30 are the residues that interact with Imatinib. Methotrexate interacts with Val23 and Lys124, and ZINC1098661 interacts with Thr22 and Lys41 residues of the protein.

Hex docking result analysis

The docking results of AgNPs & AuNPs with Irinotecan, Imatinib, Methotrexate, and ZINC1098661 targeting PDL1 receptor protein were analyzed (Table 6). The highest energy was found with AuNPs with Irinotecan to target PDL1 − 536.7 (kcal/mol). Higher energy values indicate greater stability, which implies that the interaction of Irinotecan conjugated with AuNPs is the most stable with target PDL1. The interaction of AgNPs and AuNPs with these drugs to target PDL1 is shown in (Fig. 2).

Molecular dynamics simulation analysis

A 10 ns molecular dynamics simulation was performed for PDL1 with Irinotecan, Imatinib, Methotrexate, and ZINC1098661 respectively. The parameters used to determine the stability of the simulated system are Root Mean Square Deviation (RMSD), Root Mean Square Fluctuation (RMSF), Radius of Gyration (Rg), and Solvent Accessible Surface Area (SASA). PDL1 conjugated with Irinotecan, Imatinib, and Methotrexate have a higher RMSD value than only PDL1, as shown in (Supplementary Figs. S3A, S4A, S5A, and S6A). The RMSD value for Irinotecan with PDL1 is the most stable with low fluctuation as compared to the RMSD value of Imatinib, Methotrexate, and Zinc1098661. The complex PDL1 with Irinotecan became more stable after 2500 (ps), and then a little fluctuation was observed until it reached 10,000 (ps). The overall RMSF values were similar to PDL1 and PDL1 with Irinotecan, Imatinib Methotrexate, and ZINC1098661, as shown in (Supplementary Figs. S3B, S4B, S5B, and S6B). The only region with high structural fluctuation is between atoms 1200 and 1300, which can be the site of the interaction of drugs with PDL1. The Rg values PDL1 with Irinotecan, Imatinib, Methotrexate, and ZINC1098661 are shown in (Supplementary Figs. S3C, S4C, S5C, and S6C). The Rg values of Irinotecan and

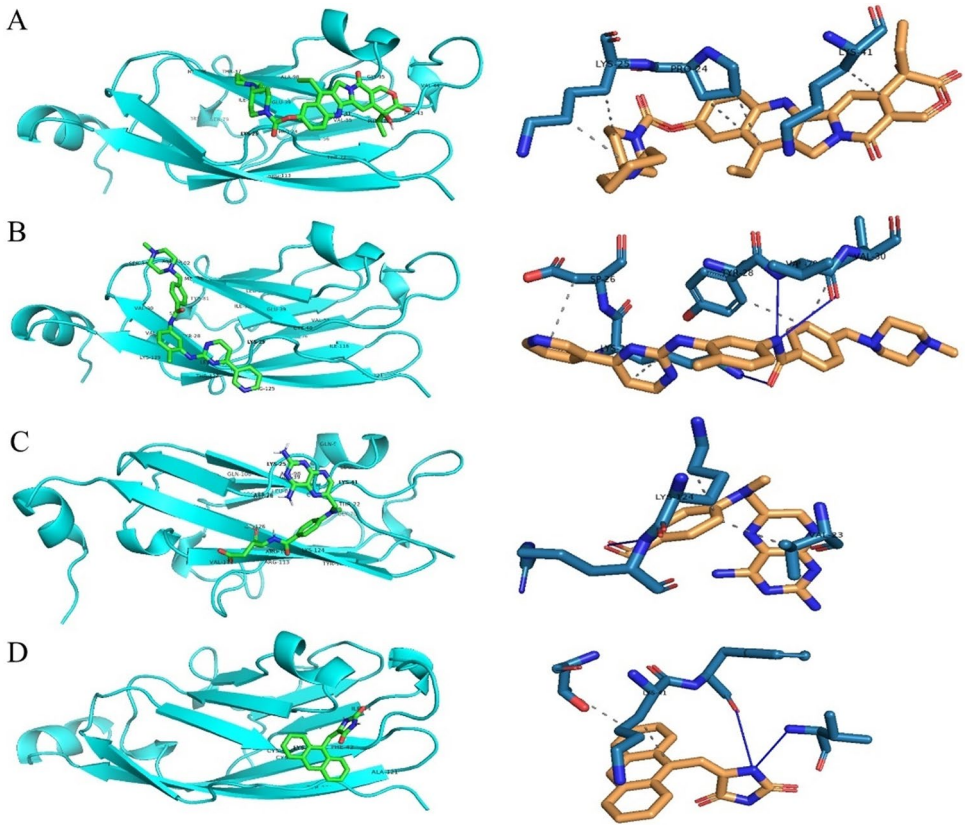

Fig. 1. Three-dimensional (3D) structural representation of PDL1 residues interacting with the compound. (**A**) Irinotecan, (**B**) Imatinib, (**C**) Methotrexate, and (**D**) ZINC1098661.

S.No.	Receptor	Compound	ETotal (kcal/mol)
1	PDL1	AgNPs with Irinotecan against PDL1	−527.2
2	PDL1	AuNPs with Irinotecan against PDL1	−536.7
3	PDL1	AgNPs with Imatinib against PDL1	−523.3
4	PDL1	AuNPs with Imatinib against PDL1	−517.3
5	PDL1	AgNPs with Methotrexate against PDL1	−506.2
6	PDL1	AuNPs with Methotrexate against PDL1	−493.3
7	PDL1	AgNPs with ZINC1098661 against PDL1	−484.0
8	PDL1	AuNPs with ZINC1098661 against PDL1	−465.5

Table 6. List of docking scores of AgNPs and AuNPs with drugs.

ZINC1098661 with PDL1 decreased over time, which indicated that the stability of the complex had increased. The Rg value of PDL1 with Imatinib increased compared to PDL1 alone, while the Rg value of PDL1 with Methotrexate showed no significant conformational change except between 5000 (ps) and 6000 (ps), which may indicate temporary conformational changes due to drug binding.

The SASA of PDL1 with Irinotecan, Imatinib, Methotrexate, and ZINC1098661 are shown in (Supplementary Figures. S3D, S4D, S5D, and S6D). The SASA of PDL1 is approximately 70 (nm^2) at 10,000(ps), while PDL1 with Irinotecan and Imatinib, SASA increased to 75 (nm^2) and 77 (nm^2) respectively. This showed that the area of PDL1 increased after drug conjugation due to the conformational changes in the protein structure. The SASA values of PDL1 with Methotrexate and ZINC1098661 decreased compared to PDL1 alone.

The stability of Irinotecan with PDL1 was further confirmed by molecular dynamics simulation for 100 ns. The analysis of RMSD value is depicted in (Fig. 3A) from 95,000(ps) to 100,000(ps). RMSD peaks of PDL1 with Irinotecan are approximately between 0.45 nm and 0.7 nm, which indicates that there was low fluctuation and the complex was stable. The high fluctuations in RMSF value were seen approximately at residue number 140, as shown in (Fig. 3B), which may be the region of protein and drug interaction. The Rg value between the period 95,000(ps) to 100,000(ps) is shown in (Fig. 3C). The Rg value of the protein and ligand complex was decreased,

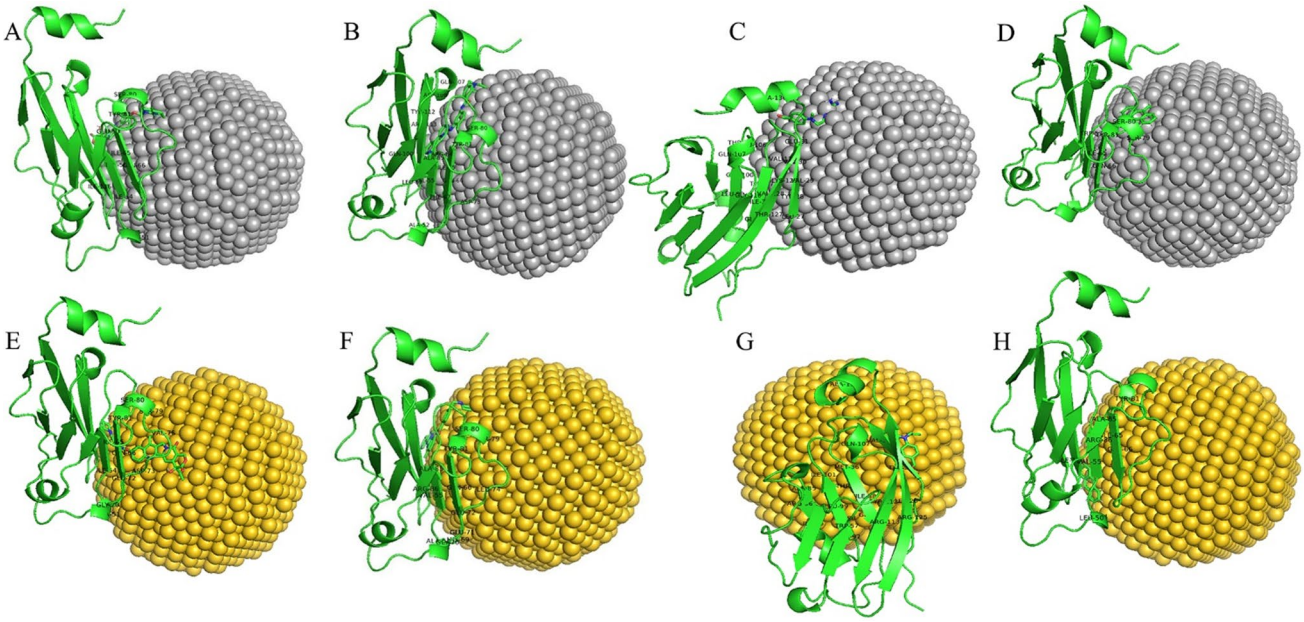

Fig. 2. Three-dimensional (3D) docked structure against PDL1. (**A**) AgNPs with Irinotecan, (**B**) AgNPs with Imatinib, (**C**) AgNPs with Methotrexate, (**D**) AgNPs with ZINC1098661, (**E**) AuNPs with Irinotecan, (**F**) AuNPs with Imatinib, (**G**) AuNPs with Methotrexate, and (**H**) AuNPs with ZINC1098661.

which confirms the stability of the complex. The SASA value of PDL1 and Irinotecan complex had increased due to the conformational changes by protein and drug interaction (Fig. 3D).

Characterization of AgNPs and AuNPs

UV–Vis analysis

The visible spectral analysis results showed that the AgNPs and AuNPs have a maximum absorbance peak of around 430 nm and 550 nm, respectively, as shown in (Fig. 4).

XRD analysis

XRD results confirmed the crystal structure of AgNPs and AuNPs. The miller indices (hkl) align with diffraction peaks of the AgNPs and AuNPs at 111, 200, 220, and 311, representing face-centered cubic (fcc) structure as shown in (Fig. 5).

FTIR analysis

In order to determine the structure of the AgNPs and AuNPs, FTIR analysis was used. In the FTIR analysis of AgNPs, as shown in (Fig. 6A), the peak at a wave number 3400 cm^{-1} indicates the presence of the OH group, and its wideness was due to the acidic OH group. The spectrum at a wave number 2100 cm^{-1} is associated with the C≡C stretching of the alkyne molecule. The peak at wave number 1650 cm^{-1} represents the C=O stretching of the carbonyl group. The peak available at 1100 cm^{-1} corresponds to the deformation vibration of the OH group. The peak available at 700 cm^{-1} is associated with CH out-of-plane bending vibrations. On analysis of FTIR of AuNPs, as shown in (Fig. 6B), the wide peak at a wave number 3400 cm^{-1} indicates the presence of the OH group that is not involved in hydrogen bonding. The spectrum available at wave number 1650 cm^{-1} represents the C=O stretching of the carbonyl group. The peaks at 1200 cm^{-1} and at 600 cm^{-1} represent ester carbonyl and C–Cl, respectively.

Characterization of AgNPs and AuNPs conjugated with drugs

UV–Vis analysis

The AgNPs and AuNPs were conjugated with three drugs (Irinotecan, Imatinib, and Methotrexate) and analyzed using a spectrophotometer. The result demonstrated a slight variation in the wavelength after conjugating AgNPs and AuNPs with these drugs, as shown in (Figs. 7 and 8).

FTIR analysis

The conjugation of AgNPs and AuNPs with drugs was confirmed using FTIR. In (Figs. 9A and 10A), the peaks observed in the Irinotecan spectrum were analyzed. The peak at 850 cm^{-1} is associated with the C–Cl stretching of a halo group. The peak available at 1150 cm^{-1} is associated with ester carbonyl, while the peak at 1400 cm^{-1} represents the CH_2 band. The peak at 1650 cm^{-1} corresponds to the C=O stretching of the carbonyl group. The peaks at 2650 and 2950 cm^{-1} correspond to C-H stretching with the presence of an aldehyde and alkane group respectively. The peak at 3400 cm^{-1} indicates the presence of an OH group. Moreover, Irinotecan peaks were also

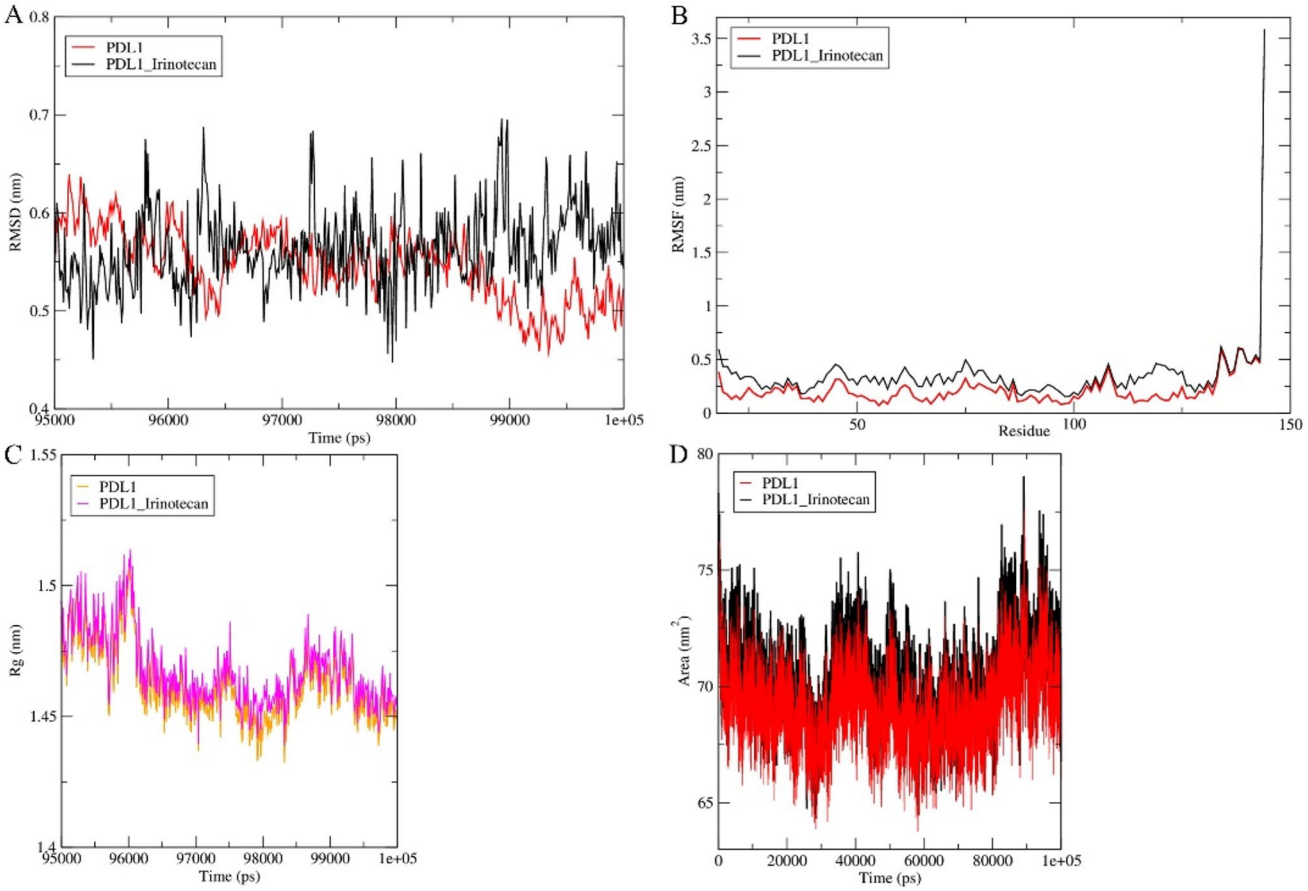

Fig. 3. (**A**) Root mean square deviation (RMSD) plot for PDL1 before and after binding with Irinotecan. (**B**) Residual fluctuations plot of PDL1 before and after interaction with Irinotecan. (**C**) Time evolution of the radius of gyration (Rg) for PDL1 and PDL1 Irinotecan Complex. (**D**) SASA as a function of time for PDL1 and Irinotecan.

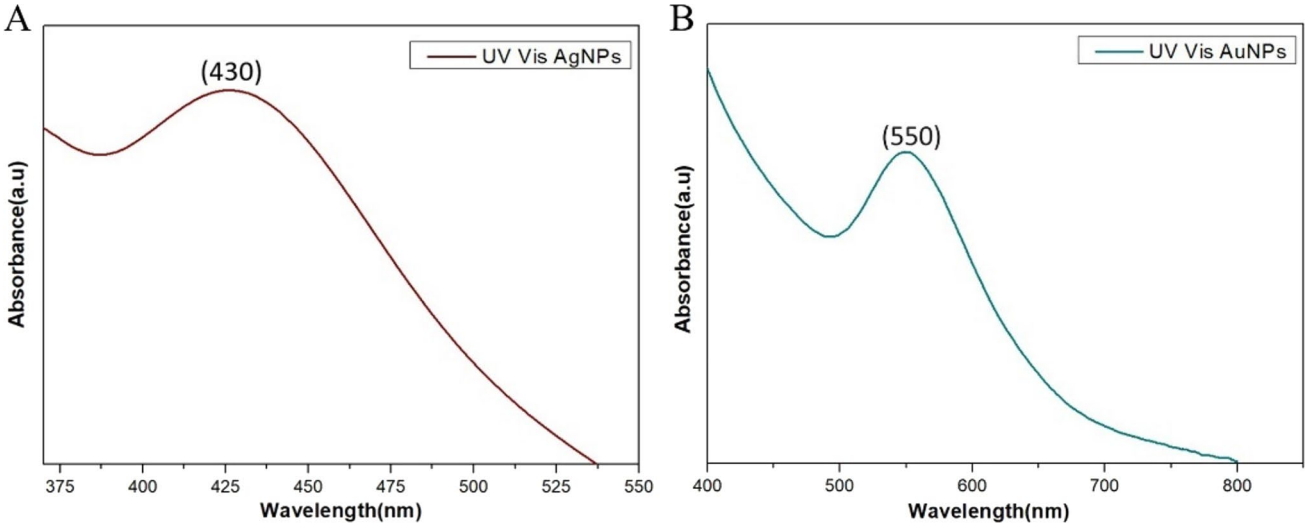

Fig. 4. The maximum absorbance peak of synthesized nanoparticles. (**A**) AgNPs, and (**B**) AuNPs.

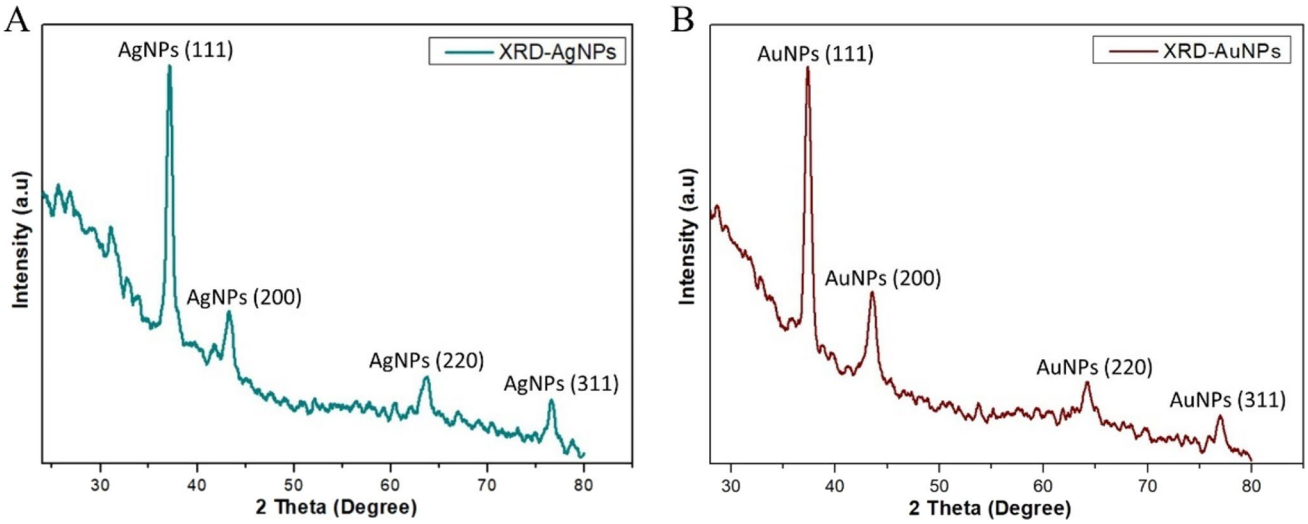

Fig. 5. XRD spectrum obtained from the synthesized nanoparticles. (**A**) AgNPs, and (**B**) AuNPs.

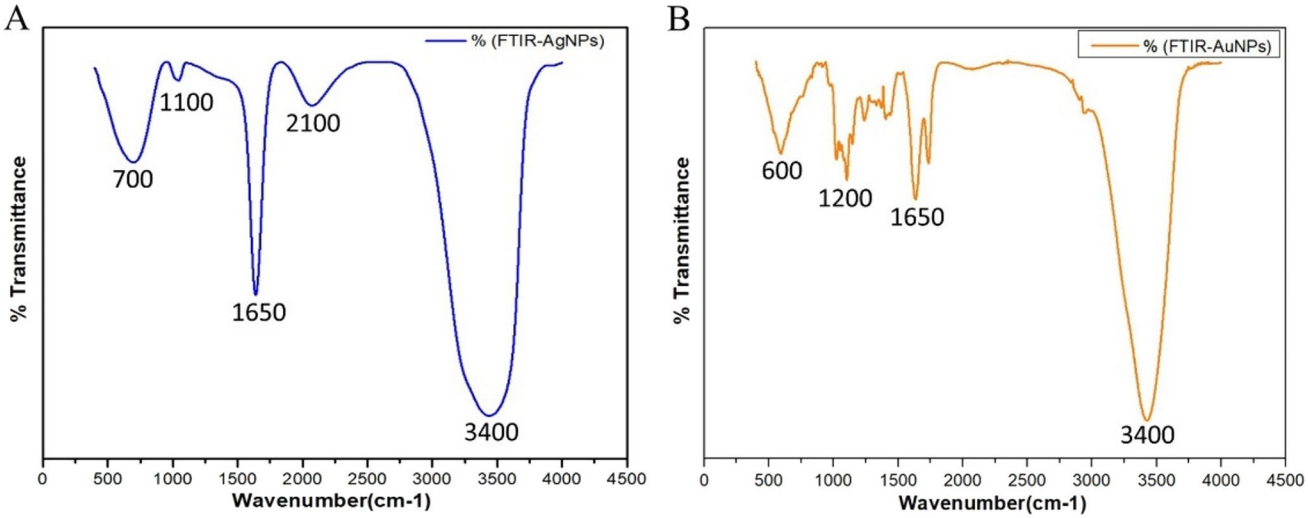

Fig. 6. The obtained FTIR result of the nanoparticles. (**A**) AgNPs, and (**B**) AuNPs.

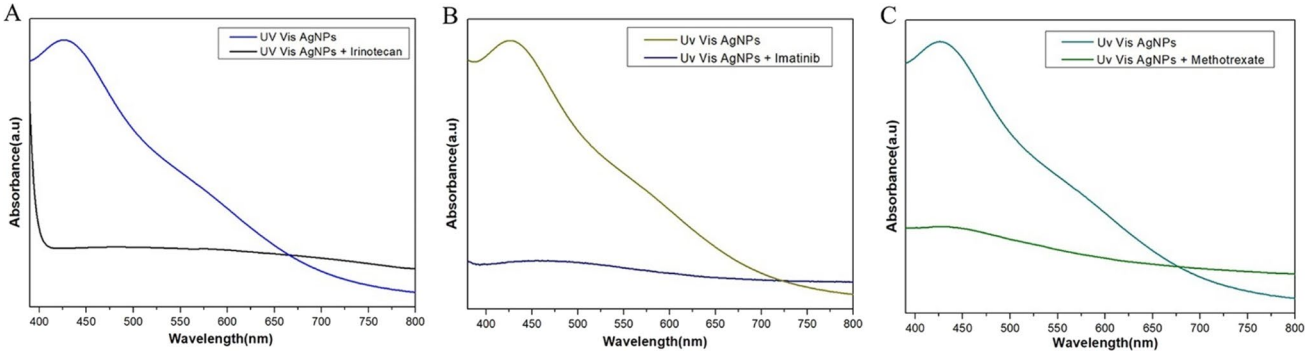

Fig. 7. Comparison of maximum absorbance peak of AgNPs with drugs. (**A**) AgNPs conjugated with Irinotecan, (**B**) AgNPs conjugated with Imatinib, and (**C**) AgNPs with Methotrexate.

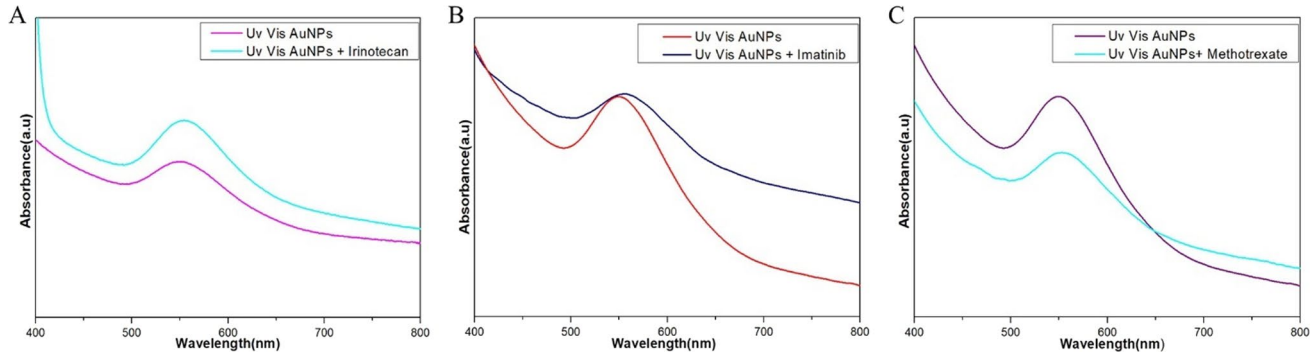

Fig. 8. Comparison of maximum absorbance peak of AuNPs with drugs. (**A**) AuNPs conjugated with Irinotecan, (**B**) AuNPs conjugated with Imatinib, and (**C**) AuNPs with Methotrexate.

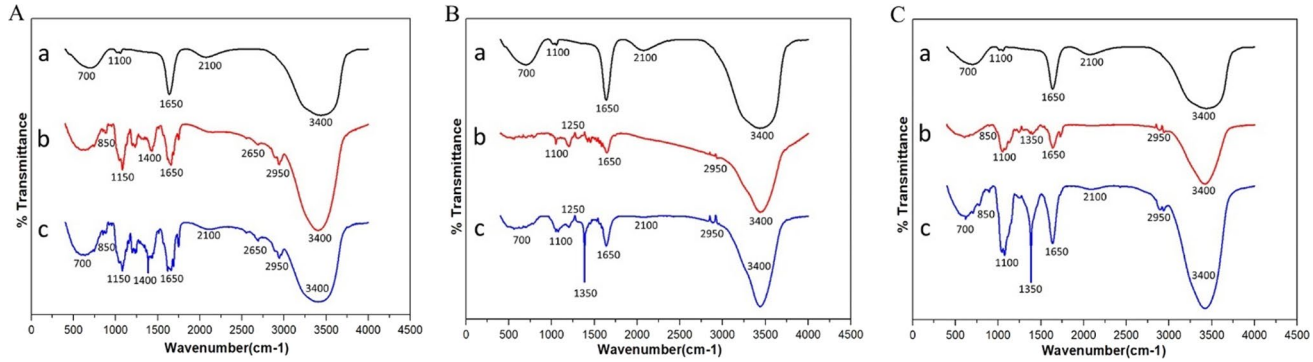

Fig. 9. (**A**) The obtained FTIR result of AgNPs and AgNPs conjugated with Irinotecan: (**a**) AgNPs, (**b**) Irinotecan, (**c**) AgNPs conjugated with Irinotecan. (**B**) The obtained FTIR result of AgNPs and AgNPs conjugated with Imatinib: (**a**) AgNPs, (**b**) Imatinib, (**c**) AgNPs conjugated with Imatinib. (**C**) The obtained FTIR result of AgNPs and AgNPs conjugated with Methotrexate: (**a**) AgNPs, (**b**) Methotrexate, (**c**) AgNPs conjugated with Methotrexate.

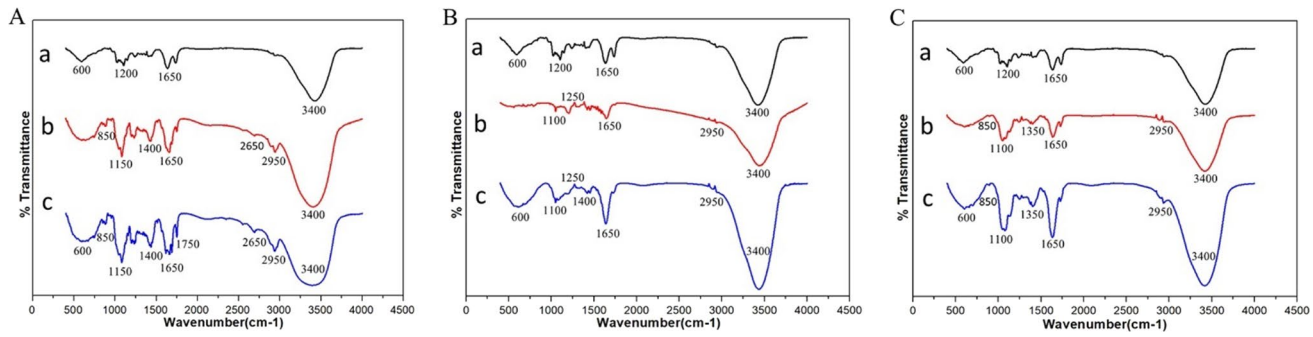

Fig. 10. (**A**) The obtained FTIR result of AuNPs and AuNPs conjugated with Irinotecan: (**a**) AuNPs, (**b**) Irinotecan, (**c**) AuNPs conjugated with Irinotecan. (**B**) The obtained FTIR result of AuNPs and AuNPs conjugated with Imatinib: (**a**) AuNPs, (**b**) Imatinib, (**c**) AuNPs conjugated with Imatinib. (**C**) The obtained FTIR result of AuNPs and AuNPs conjugated with Methotrexate: (**a**) AuNPs, (**b**) Methotrexate, (**c**) AuNPs conjugated with Methotrexate.

present in AgNPs and AuNPs conjugated with Irinotecan. Furthermore, a peak at 1750 cm^{-1} was observed in AuNPs conjugated with Irinotecan, which represents the C=C stretching of the ester group.

Imatinib FTIR spectra are demonstrated in (Figs. 9B and 10B). The peak at wave number 1100 cm^{-1} corresponds to the deformation vibration of OH. The peak at 1250 cm^{-1} is associated with the C–N stretching of the amine group, while the peak at 1650 cm^{-1} is associated with the N–H bending of the amine group. The peak available at 2950 cm^{-1} corresponds to the C–H stretching of the alkane group. The peak at 3400 cm^{-1}

indicates the presence of an OH group. These peaks were also observed in the FTIR spectra of AgNPs and AuNPs conjugated with Imatinib. In addition, in the AgNPs conjugated with Imatinib, a peak at 1350 cm^{-1} was observed, which belongs to the C–N stretching vibration of aromatic amines. Furthermore, a peak at 1400 cm^{-1}, indicative of the CH_2 band, was observed in AuNPs conjugated with Imatinib.

Methotrexate FTIR analysis is shown in (Figs. 9C and 10C). The peak at 850 cm^{-1} corresponds to the C–Cl stretching of a halo compound. The peak at 1100 cm^{-1} represents the deformation vibration of the OH group, while the peak at 1350 cm^{-1} indicates the C–N stretching vibration of aromatic amines. The peak at 1650 cm^{-1} represents the C=O stretching of the carbonyl group. The peak available at 2950 cm^{-1} corresponds to the C–H stretching of the alkane group. The peak at 3400 cm^{-1} indicates the presence of an OH group. These peaks were also observed in the FTIR spectra of AgNPs and AuNPs conjugated with Methotrexate.

Dynamic light scattering (DLS) analysis

The results obtained from Dynamic Light Scattering (DLS) indicate that the size of AgNPs and AuNPs has changed after conjugating with drugs. In particular, the average size of AgNPs was found to be 78.57 d.nm before drug conjugation (Fig. 11A). However, after conjugation with Irinotecan, Imatinib, and Methotrexate, the average size increased to 168.9, 293.2, and 220.2 d.nm, respectively, as shown in (Fig. 11B–D). Similarly, the average size of AuNPs was found to be 81.93 d.nm before drug conjugation, as demonstrated in (Fig. 12A). After conjugation with Irinotecan, Imatinib, and Methotrexate, the average size increased to 392.8, 566.9, and 562.7 d.nm, respectively, as shown in (Fig. 12B–D). This significant increase in size indicates successful conjugation of drugs with AgNPs and AuNPs. The Z-average size and Polydispersity Index (PDI) are listed in (Table 7).

In vitro analysis

The three drugs (Irinotecan, Imatinib, and Methotrexate), nanoparticles (AgNPs and AuNPs), and nanoparticles conjugated with drugs were tested on A549 cells. The MTT assay result was carried out in triplicate; the result of the MTT assay is shown in (Fig. 13).

At a drug dose of 0.5 mg/ml for Irinotecan, Imatinib, and Methotrexate, Imatinib showed high efficacy in killing cells, with cell viability of only 11%. The cell viability of Irinotecan and Methotrexate was 59.3% and 65%, respectively.

The cell viability of AgNPs and AuNPs was found to be 55.7% and 74.3%, respectively, at a concentration of 0.1 mg/ml. The AgNPs and AuNPs conjugated with drugs were tested at a concentration of 0.25 mg/ml. When AgNPs were conjugated with Irinotecan and Imatinib, the cell-killing effect of AgNPs was enhanced, with cell viability of 41.9% and 42.5%, respectively. AgNPs also enhanced the cytotoxic effect of Irinotecan but reduced it for Imatinib. When AgNPs were conjugated with Methotrexate, the effect of Methotrexate was slightly enhanced, with a cell viability of 62.3%. However, the cytotoxicity of AgNPs was reduced with Methotrexate. Conjugation of AuNPs with Irinotecan enhances the cell-killing rate. The cell viability of Irinotecan with AuNPs was 35.4%. In the case of AuNPs conjugated with Imatinib, the cell viability increased to 78.7%. Furthermore, AuNPs conjugated with Methotrexate showed a negative result in cell killing, with cell viability reaching 100%.

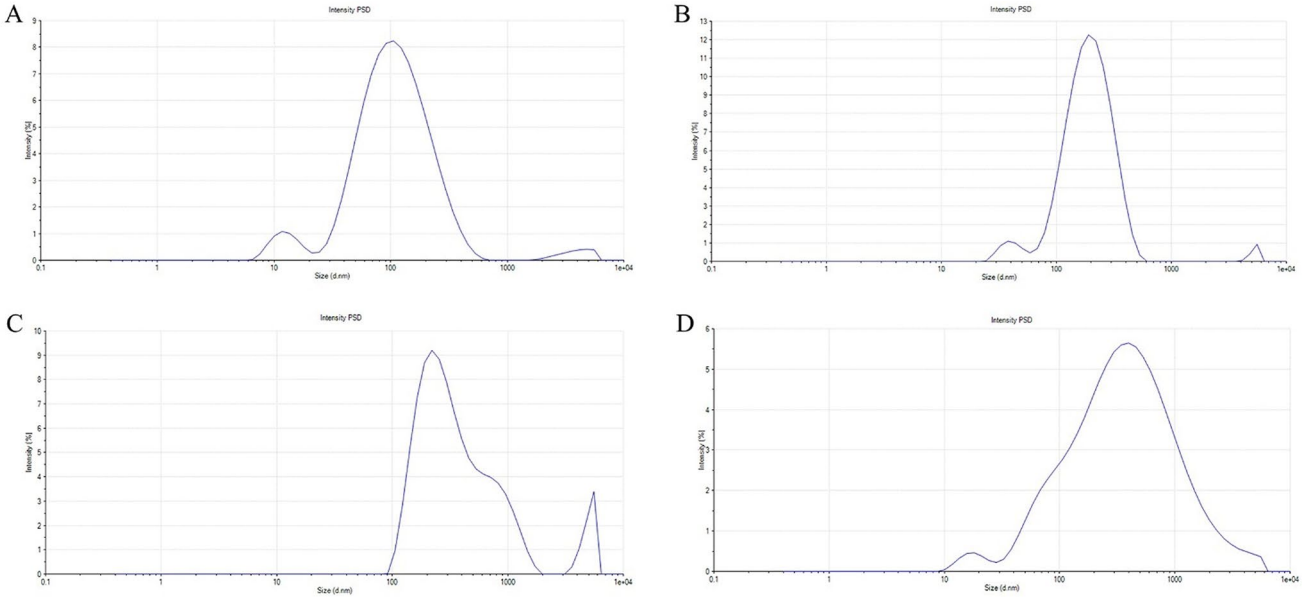

Fig. 11. DLS result of the AgNPs before and after drug conjugation. (**A**) AgNPs, (**B**) AgNPs conjugated Irinotecan, (**C**) AgNPs conjugated Imatinib, and (**D**) AgNPs conjugated Methotrexate.

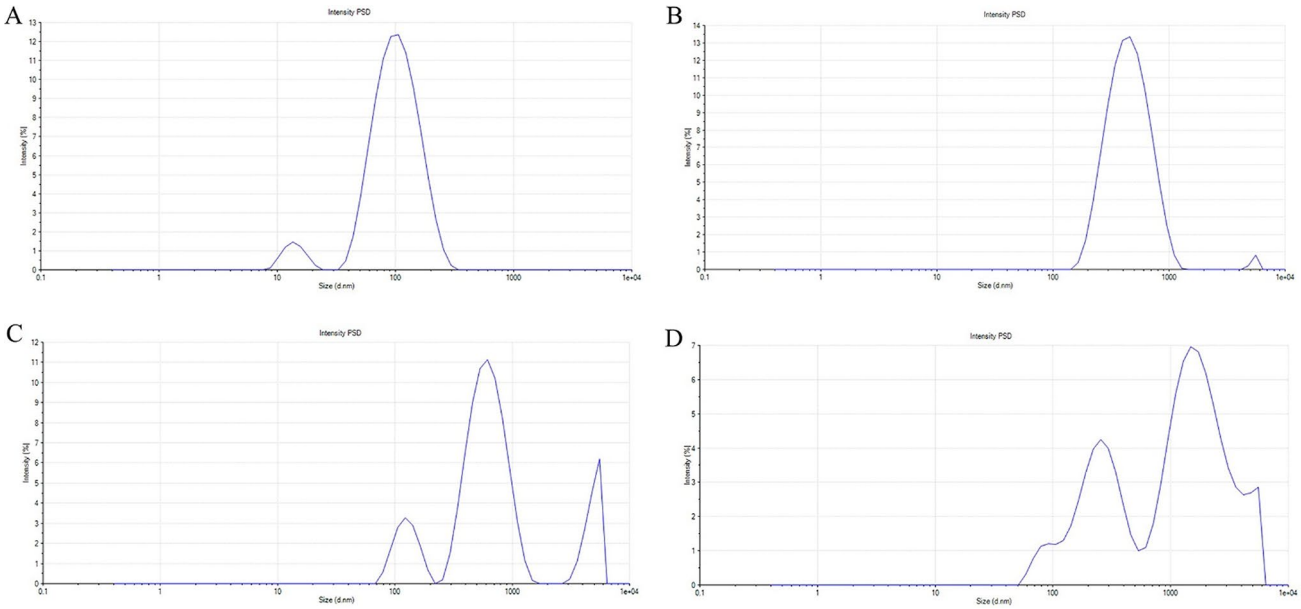

Fig. 12. DLS result of the AuNPs before and after drug conjugation. (**A**) AuNPs, (**B**) AuNPs conjugated Irinotecan, (**C**) AuNPs conjugated Imatinib, and (**D**) AuNPs conjugated Methotrexate.

S.No	Nanoparticles and Nanoparticles Drugs Conjugates	Z-average size	Polydispersity Index (PDI)
1	AgNPs	78.57 d.nm	0.295
2	AuNps	81.93 d.nm	0.272
3	AgNPs conjugated Irinotecan	168.9 d.nm	0.437
4	AgNPs conjugated Imatinib	293.2 d.nm	0.503
5	AgNPs conjugated Methotrexate	220.2 d.nm	0.547
6	AuNPs conjugated Irinotecan	392.8 d.nm	0.322
7	AuNPs conjugated Imatinib	566.9 d.nm	0.552
8	AuNPs conjugated Methotrexate	562.7 d.nm	0.600

Table 7. Z-Average Size and Polydispersity Index (PDI) of AgNPs and AuNPs and Their Conjugates with Irinotecan, Imatinib, and Methotrexate.

Discussion

Targeting the PD1/PDL1 immune checkpoint is an excellent approach in immunotherapy, which leads to the activation of T Cells[55,56].

Therefore, the aim of this work was to find a molecule that targets PDL1, which can be used with nanoparticles to inhibit the PD1/PDL1 interaction.

A two-step process was utilized in the drug screening. PyRx was used first for multiple drug screening, followed by the utilization of AutoDock Vina for further filtration. PyRx is a very robust tool that is used in various studies for multiple docking[57,58] and works on the random forest algorithm.

Afterward, AutoDock Vina was utilized to sub-filter compounds. It has been reported that Abdellah El Aissouq et al.[59] also utilized PyRx and AutoDock Vina to search for an inhibitor against SARS-CoV-2. In another study, the discovery of novel RARα agonists, the same methodology was followed[60]. AutoDock Vina works on a genetic algorithm, which is reported to perform sub-filtration after the random forest algorithm[61]. AutoDock Vina provides additional tools to add polar hydrogen atoms and Kollman charges to simulate in vivo conditions, allowing hydrogen bond interactions and electrostatic interactions between the ligand and the target molecule[62,63].

Therefore, docking score variation was noted between PyRx and AutoDock Vina. This type of trend was reported earlier, where PyRx reported affinities of −9.1 and −8.7, respectively, for Ergotamine and Simeprevir, but they changed to −7.69 and −8.5, respectively, after using AutoDock[59].

Irinotecan, Imatinib, Methotrexate, and ZINC1098661 were selected after drug screening and 3D QSAR analysis[64]. The Irinotecan had a higher affinity against PDL1 and a high experimental value. Experimental values are unitless and were obtained by Comparative Molecular Field Analysis (CoMFA) 3D QSAR methods[65], which evaluated the steric fields of drugs in relation to biological activity. The higher experimental values indicate lower

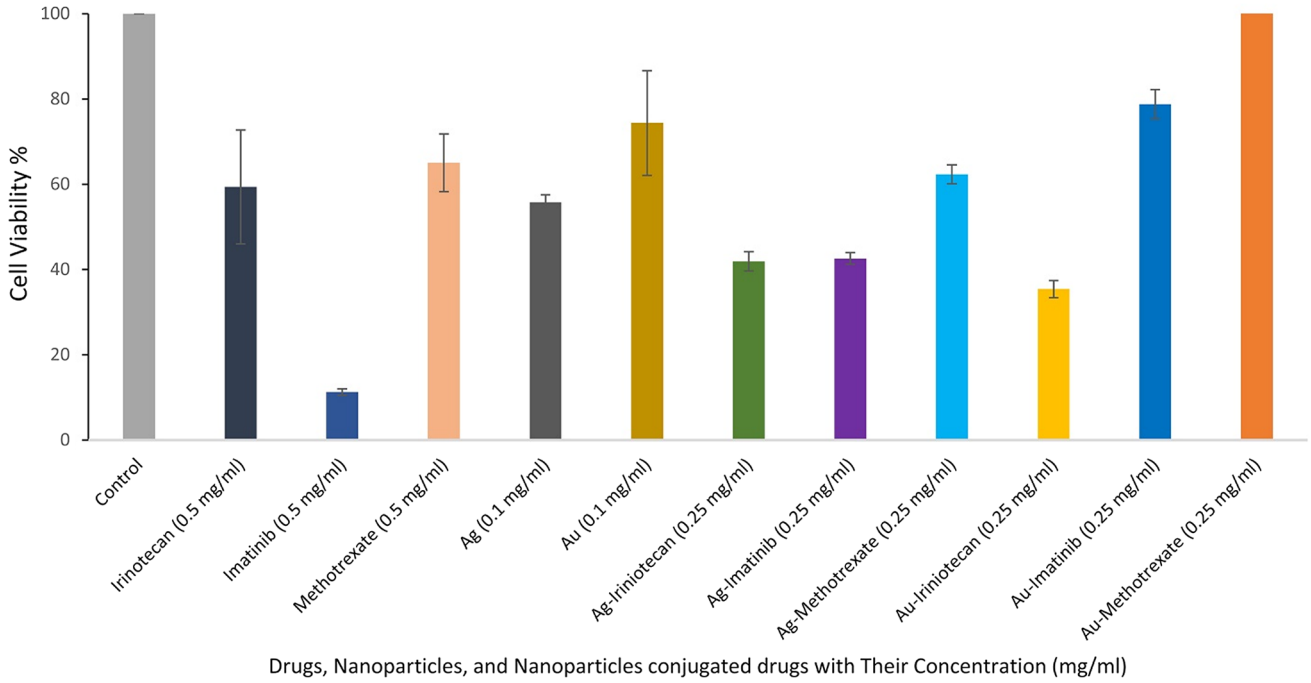

Fig. 13. The MTT assay result for A549 cells: Only drugs, AgNPs, AuNPs, and AgNPs and AuNPs conjugated with drugs.

steric hindrance between cellular components and the drugs, suggesting that the drugs can more easily enter cellular environments and interact with their targets effectively.

Moreover, ZINC1098661 with AgNPs and AuNPs had a lower affinity against PDL1; therefore, it was excluded from the wet lab experiment. Irinotecan had one violation of Lipinski's rule of five due to its weight being greater than 500 Da, but it is still considered a viable drug candidate as it is generally given intravenously. However, a study suggested that oral Irinotecan showed effective results similar to intravenous Irinotecan[66].

The GI absorption and bioavailability scores of these drugs were high, except for Methotrexate. A bioavailability score of 0.55 is considered high, as demonstrated by Bojarska et al.[67] and the majority of compounds come close to this value. In another study, Sharma et al.[68] reported that a bioavailability score of 0.11 is considered a poor score. Despite this, Methotrexate was considered in the study because of its high docking score and high experimental value analyzed by 3D QSAR. Moreover, the GI absorption and bioavailability of the Methotrexate could be improved. For example, it is reported that low doses of Methotrexate can be utilized to improve absorption[69,70]. In another study, it is demonstrated that alkalinization may greatly increase Methotrexate's solubility which can improve its bioavailability[71].

The ProTox-II analysis showed that cytotoxicity and carcinogenicity were nil with these drugs, implying that they are safe for use. Kandiah et al.[72] reported that AgNPs mediated by *Catharanthus roseus* flower extracts have a size range of 0–30 nm, characterized by a Scanning Electron Microscope (SEM). Additionally, Rabori et al.[73] study demonstrated that AuNPs mediated by *Juglans Regia* have a size range of 10 to 50 nm, characterized by Transmission Electron Microscopy (TEM). Therefore, for in silico analysis of nanoparticles, AgNPs, and AuNPs were designed arbitrarily with an average size of 35 nm according to their SEM and TEM analysis. The average size of AgNPs and AuNPs was considered the same so that the docking scores could be compared to assess their binding affinity with the drug against PDL1.

The AgNPs and AuNPs were designed using the interface force field, which is a very robust force field[74]. Hex 8.0 has been utilized for docking for AgNPs and AuNPs[75]. Hex 8.0 works on geometric hashing, which evaluates the efficiency of binding ligands on receptor sites based on shape. AuNPs with Irinotecan showed high affinity, which is due to the intrinsic properties of gold nanoparticles that allow optimal orientation for binding to the target, resulting in high affinity.

A 10 ns molecular dynamics simulation was performed to analyze the parameters, such as RMSD, RMSF, Rg, and SASA, to determine the stability of the drugs with PDL1. The higher RMSD value of PDL1 with drugs than only PDL1 indicates that the drugs induce large conformational changes in the protein structure. Overall, all the drugs were found to be stable with PDL1, but Irinotecan was found to be the most stable. Therefore, a 100 ns molecular dynamics simulation was performed specifically for Irinotecan, even though a 10 ns molecular dynamics simulation was sufficient, as demonstrated by Yu. V. Kordonskaya and his team in their research work on the behavior of tetragonal lysozyme dimer, used molecular dynamics simulation for 10 ns[76].

In RMSD, RMSF, Rg, and SASA analyses, the values for PDL1 alone were also altered because, for each simulation, there is a unique environment box in which the simulation runs for that drug. The environment box is filled with water molecules and ions to mimic an in vivo environment. The presence of the drug can alter this environment due to electrostatic interactions with the polar solvent and conformational changes in the protein

caused by drug interaction. This is also suggested by various studies where different yields of protein alone are demonstrated. For instance, RMSD values for Hemagglutinin alone vary from 3.6 to 4.8 Å. In another study, RMSD values for Hemagglutinin esterase alone vary from 3.2 to 60 Å[77,78].

Catharanthus roseus and *Juglans regia* have medicinal properties[79,80]; therefore, they were utilized for the synthesis of AgNPs and AuNPs. Since AgNPs and AuNPs were synthesized using a biological route, they had natural protein capping. Therefore, there was no need for an additional linker for drug conjugation[81], which is generally required in chemically synthesized nanoparticles.

The *Catharanthus roseus* and *Juglans regia* extracts tested on A549 cells are reported[82,83]. It was revealed that *Catharanthus roseus* showed no cytotoxic effect at 0.008% (m/v), but with an increase in concentration to 1% (m/v), cell viability decreased to 62%. *Juglans regia* showed negligible cytotoxic effect at 50 µg/mL, but at a higher concentration of 75 µg/mL, it showed a cell viability of 76%. This indicates that these extracts have no significant cytotoxic effect at low concentrations, suggesting that the nanoparticles are primarily responsible for the anti-cancer effect. However, natural extract components may contribute to enhancing the effects of nanoparticles[51,84–86].

In UV–Vis analysis, the maximum absorbance peaks of AgNPs and AuNPs were found to be 430 nm and 550 nm, respectively, due to their SPR properties. XRD confirmed the crystal structure of both AgNPs and AuNPs. The FTIR analysis showed functional groups present in them.

AgNPs and AuNPs conjugated with drugs were characterized using UV–Vis spectroscopy, FTIR, and DLS. The UV–Vis analysis showed a slight shift in the absorbance peak, indicating that drugs were conjugated[87]. Furthermore, FTIR also confirmed that AgNPs and AuNPs were conjugated with drugs[88]. DLS analysis revealed an increase in the overall size of the mixture, which also showed that the AgNPs and AuNPs were successfully conjugated with drugs[89]. DLS analysis was based on the Z-average size for the confirmation of drug conjugation; therefore, the zeta potential was not analyzed in this study.

DLS provides an average size of particles in suspension and is very sensitive to slight interactions between nanoparticles or adsorption phenomena, which can affect the hydrodynamic radius. In contrast, SEM or TEM provides individual particle sizes more accurately. Various reports show that DLS usually indicates a larger size compared to the actual size measured by SEM and TEM[51,90]. The variation in hydrodynamic radius in suspension can result in multiple peaks in DLS, as demonstrated in various reports[91–93].

In this study, A549 cells were used because they are cells of non-small cell lung cancer, which is one of the most common types of cancer with a high death rate, according to the World Health Organization (WHO). In India, lung cancer constitutes 5.9% of all cancer cases and is responsible for 8.1% of cancer deaths[94].

Moreover, various studies have been done on A549 to study the PDL1 receptor, such as studies on PDL1 expression[95], PDL1 signaling[96], and the mechanisms of PDL1 expression[97].

The MTT assay was performed to test the effect of drugs (Irinotecan, Imatinib, and Methotrexate), as well as AgNPs & AuNPs, and AgNPs & AuNPs conjugated drugs on A549 cells[98]. The MTT assay result showed that all three drugs have a toxic effect on A549 cells, among which Imatinib showed the best result. Moreover, in other studies, the toxic effect of Irinotecan, Imatinib, and Methotrexate on MCF7 cells are also reported by Saeedeh Keyvani-Ghamsari et al., Seyed Ataollah Sadat Shandiz et al., and Javad Farzanfar et al., respectively[99–101].

AgNPs were found to be more toxic than AuNPs on A549 cells. This may be due to the presence of additional anti-cancer alkaloids in AgNPs derived from *Catharanthus roseus* flowers. Yury Shkryl et al. conducted a comparative study of AgNPs and AuNPs mediated by *Lithospermum erythrorhizon*, and the result showed that the cytotoxicity of AgNPs was higher than that of AuNPs on NIH3T3 cells[102]. In other studies, the cytotoxicity of AgNPs mediated by *E. procera* and AuNPs mediated by *Lactobacillus acidophilus* were tested on MCF7 cells by Seyed Ataollah Sadat Shandiz et al. and Elmer Casley Repotente Jr. et al., respectively. Upon comparing their results, AgNPs were found to be more toxic than AuNPs[100,103,104].

The toxicity of Irinotecan, Imatinib, and Methotrexate; AgNPs and AuNPs; and the conjugated AgNPs and AuNPs with the drugs were tested at a single concentration because the purpose of this study was to test which drug's efficiency was increased with nanoparticles with low drug's concentration. Therefore, the IC_{50} value was not focused on in this study which is suggested by various studies in which the IC_{50} value was not included[105,106].

The conjugation of AgNPs with Irinotecan and Imatinib increased the toxic effect of AgNPs, whereas Methotrexate reduced the cytotoxic effect of AgNPs. Moreover, AuNPs conjugated with Irinotecan enhanced the toxic effect of AuNPs. After conjugation, the size of NPs increased, which implies that cell uptake would decrease. However, despite the increase in size, the efficiency of cell toxicity increased. This indicates a higher probability of the nanoparticles conjugated drugs binding to the cell surface receptor (PDL1).

The toxicity of Irinotecan was enhanced with AgNPs and AuNPs at low dosages, suggesting high stability of Irinotecan with AgNPs and AuNPs, which can target PDL1 effectively for treatment.

However, the toxicity of Imatinib decreased after conjugation with AgNPs & AuNPs, and AuNPs conjugated with Methotrexate were deactivated and had no effect on the A549 cells. This deactivation may be due to distortion of Methotrexate structure, which altered pharmacokinetic properties that occur after the conjugation process of Methotrexate with AuNPs[81]. This may also be due to the contrary effect of AuNPs, leading to an increase in the number of cells. The study conducted by Li et al.[107] demonstrated the proliferative effect of AuNPs on Human periodontal ligament cells (hPDLCs). Although Methotrexate was not deactivated with AgNPs, the cytotoxicity of Methotrexate slightly increased after conjugation with AgNPs.

Irinotecan showed a high affinity for PDL1, indicating that it can bind to PDL1 better than Imatinib. In vitro, Imatinib exhibited high toxicity toward A549 cells, suggesting that it is more toxic than Irinotecan. At the concentration tested, this may not be the physiologically tolerable dose form in therapy. Hence, it is necessary to study the comparison of a relevant dose of Imatinib with and without nanoparticle conjugation. However, we find Irinotecan to be a potential drug that can be benefited by the conjugation of AgNPs and AuNPs. After docking with AgNPs and AuNPs, Irinotecan conjugated with AgNPs and AuNPs showed higher affinity and

greater cytotoxicity in vitro compared to AgNPs and AuNPs conjugated with Imatinib. This suggests that AgNPs and AuNPs are efficient for targeting PDL1 and also show cytotoxicity using low dosages of Irinotecan.

Based on our current knowledge, there have been no reports regarding the targeting of PDL1 using AgNPs and AuNPs conjugated with Irinotecan, Imatinib, and Methotrexate. However, Fakhrossadat Emami et al.[24] reported that AuNPs conjugated with doxorubicin and anti-PDL1 antibodies were used to target PDL1. Our result showed that Irinotecan conjugated with AgNPs and AuNPs had a high toxic effect, which confirmed the in silico prediction for Irinotecan in which a high affinity against PDL1 was found with AgNPs and AuNPs.

In the future, a larger database of drugs can be used to discover new chemical compounds to target PDL1 receptors. Moreover, various nanoparticles such as silica shell gold core NPs and Ag-Au alloy NPs, as well as their conjugation with drugs, can be tested in various cell lines, including 3D cell lines, and also in mouse models.

Conclusion

The computational approach helped to predict the lead compound to target PDL1. 100,000 compounds were screened in silico against PDL1, and the filtered drugs were Irinotecan, Imatinib, Methotrexate, and ZINC1098661. Among these drugs, Irinotecan had a high affinity with AuNPs and AgNPs against PDL1. A molecular dynamics simulation was also performed to analyze the stability of these drugs with PDL1. Based on RMSD, RMSF, Rg, and SASA, Irinotecan with PDL1 was found to be the most stable. Furthermore, these drugs were also toxic to the A549 cells. The biological method of synthesizing AgNPs and AuNPs was simple and less expensive. Moreover, the biologically synthesized AgNPs and AuNPs had the ability to conjugate with drugs without any additional linker. The size of AgNPs and AuNPs were increased after drug conjugation. Due to their larger size, nanoparticles conjugated drugs had lower cellular penetration than nanoparticles alone. This reveals that the AgNPs and AuNPs conjugated with drugs were bound to the cell surface. The AgNPs and AuNPs also showed a toxic effect on the cell line, and the efficacy of killing cancer cells with AgNPs and AuNPs was enhanced with Irinotecan. This result suggests that AuNPs conjugated with Irinotecan can be used to target PDL1 to treat cancer. In the future, various nanoparticles such as silica shell gold core NPs and Ag-Au alloy NPs can be used to conjugate with Irinotecan and test on cell lines and mouse models.

Data availability

The original contributions presented in the study are included in the article. Further inquiries can be directed to the corresponding author.

Received: 8 July 2024; Accepted: 25 October 2024
Published online: 04 November 2024

References

1. Pucci, C., Martinelli, C. & Ciofani, G. Innovative approaches for cancer treatment: Current perspectives and new challenges. *Ecancermedicalscience* https://doi.org/10.3332/ecancer.2019.961 (2019).
2. Ferlay, J. et al. Cancer statistics for the year 2020: An overview. *Int. J. Cancer* **149**(4), 778–789. https://doi.org/10.1002/ijc.33588 (2021).
3. Wang, J., Seebacher, N., Shi, H., Kan, Q. & Duan, Z. Novel strategies to prevent the development of multidrug resistance (MDR) in cancer. *Oncotarget* **8**(48), 84559–84571. https://doi.org/10.18632/oncotarget.19187 (2017).
4. Altun, İ & Sonkaya, A. The most common side effects experienced by patients were receiving first cycle of chemotherapy. *Iran. J. Public Health* **47**(8), 1218–1219 (2018).
5. Schirrmacher, V. From chemotherapy to biological therapy: A review of novel concepts to reduce the side effects of systemic cancer treatment (Review). *Int. J. Oncol.* **54**(2), 407–419. https://doi.org/10.3892/ijo.2018.4661 (2019).
6. Wei, S. C., Duffy, C. R. & Allison, J. P. Fundamental mechanisms of immune checkpoint blockade therapy. *Cancer Discov.* **8**(9), 1069–1086. https://doi.org/10.1158/2159-8290.CD-18-0367 (2018).
7. Marin-Acevedo, J. A., Soyano, A. E., Dholaria, B., Knutson, K. L. & Lou, Y. Cancer immunotherapy beyond immune checkpoint inhibitors. *J. Hematol. Oncol.* **11**(1), 8. https://doi.org/10.1186/s13045-017-0552-6 (2018).
8. Gowd, V. et al. Advancement of cancer immunotherapy using nanoparticles-based nanomedicine. *Semin. Cancer Biol.* **86**(Pt 2), 624–644. https://doi.org/10.1016/j.semcancer.2022.03.026 (2022).
9. Liu, J. et al. PD-1/PD-L1 Checkpoint Inhibitors in Tumor Immunotherapy. *Front. Pharmacol.* **12**, 731798. https://doi.org/10.3389/fphar.2021.731798 (2021).
10. Sanmamed, M. F. & Chen, L. Inducible expression of B7–H1 (PD-L1) and its selective role in tumor site immune modulation. *Cancer J.* **20**(4), 256–261. https://doi.org/10.1097/PPO.0000000000000061 (2014).
11. Escors, D. et al. The intracellular signalosome of PD-L1 in cancer cells. *Signal Transduct. Target. Ther.* **3**(1), 26. https://doi.org/10.1038/s41392-018-0022-9 (2018).
12. Ribas, A. & Wolchok, J. D. Cancer immunotherapy using checkpoint blockade. *Science* **359**(6382), 1350–1355. https://doi.org/10.1126/science.aar4060 (2018).
13. Tran, T. H. & PhuongTran, T. T. Targeting the PD-1/PD-L1 axis for cancer treatment: A review on nanotechnology. *R. Soc. Open Sci.* https://doi.org/10.1098/rsos.211991 (2022).
14. Alharbi, B. et al. Proof of concept nanotechnological approach to in vitro targeting of malignant melanoma for enhanced immune checkpoint inhibition. *Sci. Rep.* **13**(1), 7462. https://doi.org/10.1038/s41598-023-34638-2 (2023).
15. Murthy, S. K. Nanoparticles in modern medicine: State of the art and future challenges. *Int. J. Nanomed.* **2**(2), 129–41 (2007).
16. Iravani, S., Korbekandi, H., Mirmohammadi, S. V. & Zolfaghari, B. Synthesis of silver nanoparticles: Chemical, physical and biological methods. *Res. Pharm. Sci.* **9**(6), 385–406 (2014).
17. Li, X., Xu, H., Chen, Z.-S. & Chen, G. Biosynthesis of nanoparticles by microorganisms and their applications. *J. Nanomater.* **2011**, 1–16. https://doi.org/10.1155/2011/270974 (2011).
18. Gunawardana, S. L. A. & Jayasuriya, W. J. A. B. N. Medicinally important herbal flowers in Sri Lanka. *Evid. Based. Complement. Alternat. Med.* **2019**, 2321961. https://doi.org/10.1155/2019/2321961 (2019).
19. Pham, H. N. T., Van Vuong, Q., Bowyer, M. C. & Scarlett, C. J. Phytochemicals derived from catharanthus roseus and their health benefits. *Technologies* **8**(4), 80. https://doi.org/10.3390/technologies8040080 (2020).
20. Pribis, P. Effects of walnut consumption on mood in young adults-a randomized controlled trial. *Nutrients* https://doi.org/10.3390/nu8110668 (2016).

21. Hardman, W. E. Walnuts have potential for cancer prevention and treatment in mice. *J. Nutr.* **144**(4 Suppl), 555S-560S. https://doi.org/10.3945/jn.113.188466 (2014).
22. Wang, S. & Lu, G. Applications of gold nanoparticles in cancer imaging and treatment. In *Noble and Precious Metals—Properties, Nanoscale Effects and Applications* (InTech, 2018)
23. Ivanova, N. et al. Silver nanoparticles as multi-functional drug delivery systems. In *Nanomedicines* (ed. Farrukh, M. A.) (IntechOpen, 2019).
24. Hekmat, A., Saboury, A. A. & Divsalar, A. The effects of silver nanoparticles and doxorubicin combination on DNA structure and its antiproliferative effect against T47D and MCF7 cell lines. *J. Biomed. Nanotechnol.* **8**(6), 968–982. https://doi.org/10.1166/jbn.2012.1451 (2012).
25. Emami, F. et al. Doxorubicin and Anti-PD-L1 antibody conjugated gold nanoparticles for colorectal cancer photochemotherapy. *Mol. Pharm.* **16**(3), 1184–1199. https://doi.org/10.1021/acs.molpharmaceut.8b01157 (2019).
26. Gali-Muhtasib, H. & Chouaib, R. (eds) *Nanoparticle Drug Delivery Systems for Cancer Treatment* (Jenny Stanford Publishing, 2020).
27. Liao, J., Wang, Q., Wu, F. & Huang, Z. In silico methods for identification of potential active sites of therapeutic targets. *Molecules* https://doi.org/10.3390/molecules27207103 (2022).
28. Sinha, S., Tam, B. & Wang, S. M. Applications of molecular dynamics simulation in protein study. *Membranes (Basel)* **12**(9), 844. https://doi.org/10.3390/membranes12090844 (2022).
29. Prasad, V. & Kaestner, V. Nivolumab and pembrolizumab: Monoclonal antibodies against programmed cell death-1 (PD-1) that are interchangeable. *Semin. Oncol.* **44**(2), 132–135. https://doi.org/10.1053/j.seminoncol.2017.06.007 (2017).
30. Lee, H. T. et al. Molecular mechanism of PD-1/PD-L1 blockade via anti-PD-L1 antibodies atezolizumab and durvalumab. *Sci. Rep.* **7**(1), 5532. https://doi.org/10.1038/s41598-017-06002-8 (2017).
31. Wu, Q. et al. Small molecule inhibitors targeting the PD-1/PD-L1 signaling pathway. *Acta Pharmacol. Sin.* **42**(1), 1–9. https://doi.org/10.1038/s41401-020-0366-x (2021).
32. Hernandez, I. et al. Pricing of monoclonal antibody therapies: Higher if used for cancer?. *Am. J. Manag. Care* **24**(2), 109–112 (2018).
33. Dallakyan, S. & Olson, A. J. *Small-Molecule Library Screening by Docking with PyRx* 243–250 (Springer, 2015).
34. Handoko, S. D., Ouyang, X., Su, C. T. T., Kwoh, C. K. & Ong, Y. S. QuickVina: Accelerating AutoDock Vina using gradient-based heuristics for global optimization. *IEEE/ACM Trans. Comput. Biol. Bioinforma.* **9**(5), 1266–1272. https://doi.org/10.1109/TCBB.2012.82 (2012).
35. Seeliger, D. & de Groot, B. L. Ligand docking and binding site analysis with PyMOL and Autodock/Vina. *J. Comput. Aided. Mol. Des.* **24**(5), 417–422. https://doi.org/10.1007/s10822-010-9352-6 (2010).
36. Ragno, R. et al. Teaching and learning computational drug design: Student investigations of 3D quantitative structure-activity relationships through web applications. *J. Chem. Educ.* **97**(7), 1922–1930. https://doi.org/10.1021/acs.jchemed.0c00117 (2020).
37. Mendez, D. et al. ChEMBL: Towards direct deposition of bioassay data. *Nucleic Acids Res.* **47**(D1), D930–D940. https://doi.org/10.1093/nar/gky1075 (2019).
38. Jo, S., Kim, T., Iyer, V. G. & Im, W. CHARMM-GUI: A web-based graphical user interface for CHARMM. *J. Comput. Chem.* **29**(11), 1859–1865. https://doi.org/10.1002/jcc.20945 (2008).
39. Ghoorah, A. W., Devignes, M.-D., Smaïl-Tabbone, M. & Ritchie, D. W. Protein docking using case-based reasoning. *Proteins Struct. Funct. Bioinforma.* **81**(12), 2150–2158. https://doi.org/10.1002/prot.24433 (2013).
40. Daina, A., Michielin, O. & Zoete, V. SwissADME: A free web tool to evaluate pharmacokinetics, drug-likeness and medicinal chemistry friendliness of small molecules. *Sci. Rep.* **7**(1), 42717. https://doi.org/10.1038/srep42717 (2017).
41. Banerjee, P., Eckert, A. O., Schrey, A. K. & Preissner, R. ProTox-II: A webserver for the prediction of toxicity of chemicals. *Nucleic Acids Res.* **46**(W1), W257–W263. https://doi.org/10.1093/nar/gky318 (2018).
42. Schüttelkopf, A. W. & van Aalten, D. M. F. PRODRG: A tool for high-throughput crystallography of protein-ligand complexes. *Acta Crystallogr. D. Biol. Crystallogr.* **60**(Pt 8), 1355–1363. https://doi.org/10.1107/S0907444904011679 (2004).
43. Pol-Fachin, L., Fernandes, C. L. & Verli, H. GROMOS96 43a1 performance on the characterization of glycoprotein conformational ensembles through molecular dynamics simulations. *Carbohydr. Res.* **344**(4), 491–500. https://doi.org/10.1016/j.carres.2008.12.025 (2009).
44. Kagami, L. P. et al. LiGRO: A graphical user interface for protein-ligand molecular dynamics. *J. Mol. Model.* **23**(11), 304. https://doi.org/10.1007/s00894-017-3475-9 (2017).
45. de Souza, O. N. & Ornstein, R. L. Effect of periodic box size on aqueous molecular dynamics simulation of a DNA dodecamer with particle-mesh Ewald method. *Biophys. J.* **72**(6), 2395–2397. https://doi.org/10.1016/S0006-3495(97)78884-2 (1997).
46. Humphrey, W., Dalke, A. & Schulten, K. VMD: Visual molecular dynamics. *J. Mol. Graph.* **14**(1), 33–8. https://doi.org/10.1016/0263-7855(96)00018-5 (1996).
47. Soman, S. S., Sivakumar, K. C. & Sreekumar, E. Molecular dynamics simulation studies and in vitro site directed mutagenesis of avian beta-defensin Apl_AvBD2. *BMC Bioinform.* **11**(Suppl 1), S7. https://doi.org/10.1186/1471-2105-11-S1-S7 (2010).
48. AboElmaaty, S. A. et al. Biofilm inhibitory activity of actinomycete-synthesized agnps with low cytotoxic effect: Experimental and in silico study. *Microorganisms* https://doi.org/10.3390/microorganisms11010102 (2022).
49. Tan, Y., Liu, L., Wang, Y. & Liu, J. pH-regulated surface plasmon absorption from ultrasmall luminescent gold nanoparticles. *Adv. Opt. Mater.* **6**(10), 1701324. https://doi.org/10.1002/adom.201701324 (2018).
50. Mourdikoudis, S., Pallares, R. M. & Thanh, N. T. K. Characterization techniques for nanoparticles: Comparison and complementarity upon studying nanoparticle properties. *Nanoscale* **10**(27), 12871–12934. https://doi.org/10.1039/C8NR02278J (2018).
51. Moosavy, M.-H. et al. Green synthesis, characterization, and biological evaluation of gold and silver nanoparticles using Mentha spicata essential oil. *Sci. Rep.* **13**(1), 7230. https://doi.org/10.1038/s41598-023-33632-y (2023).
52. Liu, Y. et al. pH-driven reversible assembly and disassembly of colloidal gold nanoparticles. *Front. Chem.* https://doi.org/10.3389/fchem.2021.675491 (2021).
53. Tiernan, H., Byrne, B. & Kazarian, S. G. ATR-FTIR spectroscopy and spectroscopic imaging for the analysis of biopharmaceuticals. *Spectrochim. Acta. A. Mol. Biomol. Spectrosc.* **241**, 118636. https://doi.org/10.1016/j.saa.2020.118636 (2020).
54. Bhattacharjee, S. DLS and zeta potential—What they are and what they are not?. *J. Control. Release* **235**, 337–351. https://doi.org/10.1016/j.jconrel.2016.06.017 (2016).
55. Shi, L., Chen, S., Yang, L. & Li, Y. The role of PD-1 and PD-L1 in T-cell immune suppression in patients with hematological malignancies. *J. Hematol. Oncol.* **6**(1), 74. https://doi.org/10.1186/1756-8722-6-74 (2013).
56. Acúrcio, R. C. et al. Therapeutic targeting of PD-1/PD-L1 blockade by novel small-molecule inhibitors recruits cytotoxic T cells into solid tumor microenvironment. *J. Immunother. Cancer* **10**(7), e004695. https://doi.org/10.1136/jitc-2022-004695 (2022).
57. de Sousa, A. C. C., Combrinck, J. M., Maepa, K. & Egan, T. J. Virtual screening as a tool to discover new β-haematin inhibitors with activity against malaria parasites. *Sci. Rep.* **10**(1), 3374. https://doi.org/10.1038/s41598-020-60221-0 (2020).
58. Da, A., Wu-Lu, M., Dragelj, J., Mroginski, M. A. & Ebrahimi, K. H. Multi-structural molecular docking (MOD) combined with molecular dynamics reveal the structural requirements of designing broad-spectrum inhibitors of SARS-CoV-2 entry to host cells. *Sci. Rep.* **13**(1), 16387. https://doi.org/10.1038/s41598-023-42015-2 (2023).
59. El Aissouq, A., Chedadi, O., Bouachrine, M. & Ouammou, A. Identification of Novel SARS-CoV-2 Inhibitors: A structure-based virtual screening approach. *J. Chem.* **2021**, 1–7. https://doi.org/10.1155/2021/1901484 (2021).

60. Ghorayshian, A., Danesh, M., Mostashari-Rad, T. & Fassihi, A. Discovery of novel RARα agonists using pharmacophore-based virtual screening, molecular docking, and molecular dynamics simulation studies. *PLoS One* **18**(8), e0289046. https://doi.org/10.1371/journal.pone.0289046 (2023).
61. Saqib, P., Qamar, U., Aslam, A. & Ahmad, A. Hybrid of filters and genetic algorithm—random forests based wrapper approach for feature selection and prediction. pp. 190–199 (2019).
62. Xue, Q. et al. Evaluation of the binding performance of flavonoids to estrogen receptor alpha by Autodock, Autodock Vina and Surflex-Dock. *Ecotoxicol. Environ. Saf.* **233**, 113323. https://doi.org/10.1016/j.ecoenv.2022.113323 (2022).
63. Azad, I. et al. Identification of severe acute respiratory syndrome coronavirus-2 inhibitors through in silico structure-based virtual screening and molecular interaction studies. *J. Mol. Recognit.* **34**(10), e2918. https://doi.org/10.1002/jmr.2918 (2021).
64. Rasulev, B. Recent developments in 3D QSAR and molecular docking studies of organic and nanostructures. In *Handbook of Computational Chemistry* (eds Leszczynski, J. et al.) 2133–2161 (Springer, 2017).
65. Fang, Y. et al. 3D-QSAR and docking studies of flavonoids as potent Escherichia coli inhibitors. *Sci. Rep.* **6**(1), 23634. https://doi.org/10.1038/srep23634 (2016).
66. Kümler, I. et al. Oral administration of irinotecan in patients with solid tumors: An open-label, phase I, dose escalating study evaluating safety, tolerability and pharmacokinetics. *Cancer Chemother. Pharmacol.* **83**(1), 169–178. https://doi.org/10.1007/s00280-018-3720-7 (2019).
67. Bojarska, J. et al. A supramolecular approach to structure-based design with a focus on synthons hierarchy in ornithine-derived ligands: Review, synthesis, experimental and in silico studies. *Molecules* **25**(5), 1135. https://doi.org/10.3390/molecules25051135 (2020).
68. Sharma, P. & Shanavas, A. Natural derivatives with dual binding potential against SARS-CoV-2 main protease and human ACE2 possess low oral bioavailability: A brief computational analysis. *J. Biomol. Struct. Dyn.* **39**(15), 5819–5830. https://doi.org/10.1080/07391102.2020.1794970 (2021).
69. van Roon, E. N. & van de Laar, M. A. F. J. Methotrexate bioavailability. *Clin. Exp. Rheumatol.* **28**(5 Suppl 61), S27-32 (2010).
70. Colleoni, M. et al. Low-dose oral methotrexate and cyclophosphamide in metastatic breast cancer: Antitumor activity and correlation with vascular endothelial growth factor levels. *Ann. Oncol.* **13**(1), 73–80. https://doi.org/10.1093/annonc/mdf013 (2002).
71. Howard, S. C., McCormick, J., Pui, C.-H., Buddington, R. K. & Harvey, R. D. Preventing and managing toxicities of high-dose methotrexate. *Oncologist* **21**(12), 1471–1482. https://doi.org/10.1634/theoncologist.2015-0164 (2016).
72. Kandiah, M. & Chandrasekaran, K. N. Green synthesis of silver nanoparticles using *Catharanthus roseus* flower extracts and the determination of their antioxidant, antimicrobial, and photocatalytic activity. *J. Nanotechnol.* **2021**, 1–18. https://doi.org/10.1155/2021/5512786 (2021).
73. Rabori, M. S., Karimabad, M. N. & Hajizadeh, M. R. Facile, low-cost and rapid phytosynthesis of stable and eco-friendly gold nanoparticles using green walnut shell and study of their anticancer potential. *World Cancer Res. J.* **8**, 1–8 (2021).
74. Choi, Y. K. et al. CHARMM-GUI nanomaterial modeler for modeling and simulation of nanomaterial systems. *J. Chem. Theory Comput.* **18**(1), 479–493. https://doi.org/10.1021/acs.jctc.1c00996 (2022).
75. Mohanty, M. & Mohanty, P. S. Molecular docking in organic, inorganic, and hybrid systems: A tutorial review. *Monatshefte für Chemie Chem. Mon.* **154**(7), 683–707. https://doi.org/10.1007/s00706-023-03076-1 (2023).
76. Kordonskaya, Y. V. et al. Effect of the simulation box size and precipitant concentration on the behavior of tetragonal lysozyme dimer. *Crystallogr. Rep.* **66**(3), 525–528. https://doi.org/10.1134/S106377452103010X (2021).
77. Bordoloi, S. et al. Structure-based virtual screening and molecular dynamic simulations identified FDA-approved molecules as potential inhibitors against the surface proteins of H1N1. *bioRxiv* https://doi.org/10.1101/2023.12.02.569695 (2023).
78. Patel, C. N., Kumar, S. P., Pandya, H. A. & Rawal, R. M. Identification of potential inhibitors of coronavirus hemagglutinin-esterase using molecular docking, molecular dynamics simulation and binding free energy calculation. *Mol. Divers.* **25**(1), 421–433. https://doi.org/10.1007/s11030-020-10135-w (2021).
79. JairBarrales-Cureño, H. et al. Alkaloids of pharmacological importance in *Catharanthus roseus*. In *Alkaloids—Their Importance in Nature and Human Life* (ed. Kurek, J.) (IntechOpen, 2019).
80. Mateş, L., Rusu, M. E. & Popa, D.-S. Phytochemicals and biological activities of walnut septum: A systematic review. *Antioxidants* **12**(3), 604. https://doi.org/10.3390/antiox12030604 (2023).
81. Yahyaei, B. & Pourali, P. One step conjugation of some chemotherapeutic drugs to the biologically produced gold nanoparticles and assessment of their anticancer effects. *Sci. Rep.* **9**(1), 10242. https://doi.org/10.1038/s41598-019-46602-0 (2019).
82. Gumy, M. N., Kanunfre, C. C., Padilha, J. D. P., Cruz, L. S. & Boscardin, P. M. D. Silver nanoparticles green synthesis from *Catharanthus roseus* flowers and effect on A549 lung cancer cells. *Brazilian Arch. Biol. Technol.* https://doi.org/10.1590/1678-4324-ssbfar-2023220989 (2023).
83. Rusu, M. E. et al. Walnut (*Juglans regia* L.) septum: Assessment of bioactive molecules and in vitro biological effects. *Molecules* **25**(9), 2187. https://doi.org/10.3390/molecules25092187 (2020).
84. Ansari, M. et al. Plant mediated fabrication of silver nanoparticles, process optimization, and impact on tomato plant. *Sci. Rep.* **13**(1), 18048. https://doi.org/10.1038/s41598-023-45038-x (2023).
85. Ullah, Z. et al. Biogenic synthesis, characterization, and in vitro biological investigation of silver oxide nanoparticles (AgONPs) using Rhynchosia capitata. *Sci. Rep.* **14**(1), 10484. https://doi.org/10.1038/s41598-024-60694-3 (2024).
86. Muddapur, U. M. et al. Plant-based synthesis of gold nanoparticles and theranostic applications: A review. *Molecules* **27**(4), 1391. https://doi.org/10.3390/molecules27041391 (2022).
87. Mohd-Zahid, M. H. et al. Gold nanoparticles conjugated with anti-CD133 monoclonal antibody and 5-fluorouracil chemotherapeutic agent as nanocarriers for cancer cell targeting. *RSC Adv.* **11**(26), 16131–16141. https://doi.org/10.1039/D1RA01093J (2021).
88. Ravasco, J. M. J. M., Faustino, H., Trindade, A. & Gois, P. M. P. Bioconjugation with maleimides: A useful tool for chemical biology. *Chemistry* **25**(1), 43–59. https://doi.org/10.1002/chem.201803174 (2019).
89. Mohamed, H. E., Mohamed, A. A., Al-Ghobashy, M. A., Fathalla, F. A. & Abbas, S. S. Stability assessment of antibody-drug conjugate Trastuzumab emtansine in comparison to parent monoclonal antibody using orthogonal testing protocol. *J. Pharm. Biomed. Anal.* **150**, 268–277. https://doi.org/10.1016/j.jpba.2017.12.022 (2018).
90. Keijok, W. J. et al. Controlled biosynthesis of gold nanoparticles with Coffea arabica using factorial design. *Sci. Rep.* **9**(1), 16019. https://doi.org/10.1038/s41598-019-52496-9 (2019).
91. Singh, K., Panghal, M., Kadyan, S., Chaudhary, U. & Yadav, J. P. Green silver nanoparticles of *Phyllanthus amarus*: As an antibacterial agent against multi drug resistant clinical isolates of Pseudomonas aeruginosa. *J. Nanobiotechnol.* **12**(1), 40. https://doi.org/10.1186/s12951-014-0040-x (2014).
92. Srinath, B. S. & Ravishankar Rai, V. Biosynthesis of highly monodispersed, spherical gold nanoparticles of size 4–10 nm from spent cultures of Klebsiella pneumoniae. *3 Biotech* **5**(5), 671–676. https://doi.org/10.1007/s13205-014-0265-2 (2015).
93. Caputo, F., Clogston, J., Calzolai, L., Rösslein, M. & Prina-Mello, A. Measuring particle size distribution of nanoparticle enabled medicinal products, the joint view of EUNCL and NCI-NCL. A step by step approach combining orthogonal measurements with increasing complexity. *J. Control. Release* **299**, 31–43. https://doi.org/10.1016/j.jconrel.2019.02.030 (2019).
94. Singh, N. et al. Lung cancer in India. *J. Thorac. Oncol.* **16**(8), 1250–1266. https://doi.org/10.1016/j.jtho.2021.02.004 (2021).
95. Ou, Z., Dou, X., Tang, N. & Liu, G. Pressure increases PD-L1 expression in A549 lung adenocarcinoma cells and causes resistance to anti-ROR1 CAR T cell-mediated cytotoxicity. *Sci. Rep.* **12**(1), 6919. https://doi.org/10.1038/s41598-022-10905-6 (2022).

96. Li, T. et al. Exploring a tumor-intrinsic PD-L1 signal with proximity-dependent biotin identification in lung cancer cells. *Biochemistry* **58**(18), 2293–2296. https://doi.org/10.1021/acs.biochem.9b00113 (2019).
97. Li, F. et al. Preliminary mechanisms of regulating PD-L1 expression in non-small cell lung cancer during the EMT process. *Oncol. Rep.* https://doi.org/10.3892/or.2018.6474 (2018).
98. Kumar, P., Nagarajan, A. & Uchil, P. D. Analysis of cell viability by the MTT assay. *Cold Spring Harb. Protoc.* **2018**(6), pdb. prot095505. https://doi.org/10.1101/pdb.prot095505 (2018).
99. Keyvani-Ghamsari, S., Rabbani-Chadegani, A., Sargolzaei, J. & Shahhoseini, M. Effect of irinotecan on HMGB1, MMP9 expression, cell cycle, and cell growth in breast cancer (MCF-7) cells. *Tumor Biol.* **39**(4), 101042831769835. https://doi.org/10.1177/1010428317698354 (2017).
100. Sadat Shandiz, S. A. et al. Novel imatinib-loaded silver nanoparticles for enhanced apoptosis of human breast cancer MCF-7 cells. *Artif. Cells Nanomed. Biotechnol.* **45**(6), 1082–1091. https://doi.org/10.1080/21691401.2016.1202257 (2017).
101. Farzanfar, J., Farjadian, F., Roointan, A., Mohammadi-Samani, S. & Tayebi, L. Assessment of pH responsive delivery of methotrexate based on PHEMA-st-PEG-DA Nanohydrogels. *Macromol. Res.* **29**(1), 54–61. https://doi.org/10.1007/s13233-021-9007-6 (2021).
102. Shkryl, Y. et al. Biosynthesis and cytotoxic properties of Ag, Au, and bimetallic nanoparticles synthesized using lithospermum erythrorhizon callus culture extract. *Int. J. Mol. Sci.* **22**(17), 9305. https://doi.org/10.3390/ijms22179305 (2021).
103. Repotente, E. C., Carreon, A. J., Devanadera, M. K., Esmalla, M. S. & Santiago-Bautista, M. Cytotoxic potential on human breast and lung cancer cells of the biosynthesized gold nanoparticles from the reduction of chloroauric acid by lactic acid isolated from Lactobacillus acidophilus. *Front. Mater.* https://doi.org/10.3389/fmats.2022.933749 (2022).
104. Peivandi, Z. et al. Silica nanoparticles-induced cytotoxicity and genotoxicity in A549 cell lines. *Sci. Rep.* **14**(1), 1–8. https://doi.org/10.1038/s41598-024-65333-5 (2024).
105. Esfandyari-Manesh, M. et al. Improved anticancer delivery of paclitaxel by albumin surface modification of PLGA nanoparticles. *DARU J. Pharm. Sci.* **23**(1), 28. https://doi.org/10.1186/s40199-015-0107-8 (2015).
106. Jiang, X. et al. Nanotoxicity of silver nanoparticles on HEK293T cells: A combined study using biomechanical and biological techniques. *ACS Omega* **3**(6), 6770–6778. https://doi.org/10.1021/acsomega.8b00608 (2018).
107. Li, C., Li, Z., Wang, Y. & Liu, H. Gold nanoparticles promote proliferation of human periodontal ligament stem cells and have limited effects on cells differentiation. *J. Nanomater.* **2016**, 1–10. https://doi.org/10.1155/2016/1431836 (2016).

Acknowledgements

We would like to express our gratitude Prof. Mohammad Owais (Interdisciplinary Biotechnology Unit, AMU) for helping in MTT assay, Dr. Snober S. Mir (Department of Bioengineering, Integral University) for providing cell line. We acknowledge the laboratory assistance provided by Mr. Khateeb Ahmad (INC), Mr. Ashraf Ali (INC), and Mr. Syed Danish Ali (Department of Applied physics, AMU) in the characterization of samples. We thank Drs. Suhail Akhtar and Abdul Malik for their valuable suggestions and reviewing the contents.

Author contributions

M.A.A. conceived the study, planned experiments, provided resources, discussed results, analyzed data, and helped write the manuscript. S.H.A. did experimental work and wrote the manuscript draft. H.A. analyzed data and helped in manuscript writing and discussion. All authors contributed to the article and approved the submitted version.

Funding

This work was supported and funded by Aligarh Muslim University, Aligarh, India.

Declarations

Competing interests

The authors declare no competing interests.

Ethics approval and consent to participate

Not applicable.

Consent for publication

Not applicable.

Additional information

Supplementary Information The online version contains supplementary material available at https://doi.org/10.1038/s41598-024-77868-8.

Correspondence and requests for materials should be addressed to M.A.A.

Reprints and permissions information is available at www.nature.com/reprints.

Publisher's note Springer Nature remains neutral with regard to jurisdictional claims in published maps and institutional affiliations.